BM@N Note

Production of *Λ* hyperons in interactions of the 4A GeV carbon beam with *C, Al, Cu* targets.

Analysis team: Yu.Gornaya, M.Kapishin, G.Pokatashkin, I.Rufanov, V.Vasendina, A.Zinchenko

Abstract

Production of *Λ* hyperons in interactions of the 4 GeV kinetic energy carbon beam with *C, Al, Cu* targets was studied with the BM@M detector at the Nuclotron (LHEP JINR, Dubna).The analysis procedure is described in details. Results on *Λ* hyperon yields have been obtained and compared with model predictions and data available.

BM@N configuration in the carbon beam run

The technical run of the BM@N detector was performed with the carbon beam in March 2017. The view of the BM@N setup used in the run is presented in Fig. 1 (left). The configuration of the central tracker was based on one plane of a forward silicon detector and six GEM stations combined from 5 GEM detectors with the size of 66x41 cm^2 and 2 GEM detectors with the size of 163x45 cm^2 [GEMTDR]. The tracking stations were arranged to have the beam passing through their centers (Fig. 1 (right)). Each successive GEM station was rotated by 180^o around the vertical axis. It was done to have the opposite electron drift direction in the successive stations in order to avoid a systematic shift of reconstructed tracks due to the Lorentz angle in the magnetic field. The research program was devoted to measurements of inelastic reactions *C+A→X* with the beam kinetic energy of 3.5, 4 and 4.5A GeV and different targets: *C, Al, Cu*. In the present analysis only data collected in the 4A GeV carbon beam are considered. The technical program of the run included the measurement of the carbon beam momentum in the central and outed tracker at different values of the magnetic field. Since the GEM tracker configuration was tuned to measure relatively high-momentum beam particles, the geometric acceptance for relatively soft decay products of strange *V0* particles was rather low.

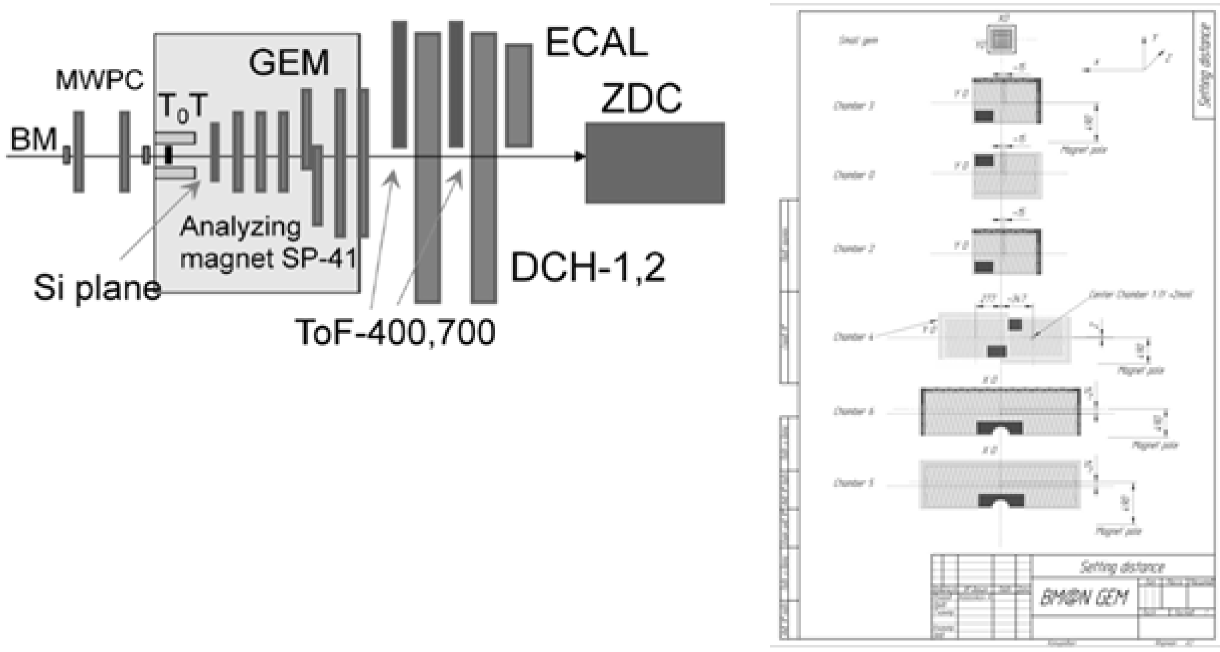

Fig. 1. Left plot: BM@N set-up in the carbon beam run. Right plot: configuration of the GEM detectors.

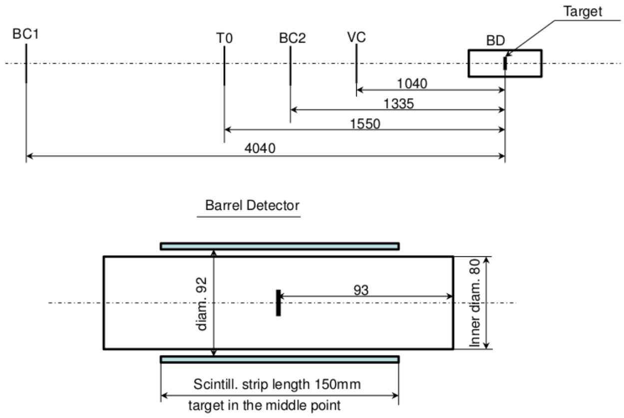

Fig.1b. Schematic view and positions of the beam counters, barrel detector and target.

In the present analysis the experimental data from the forward silicon detector, GEM detectors, trigger barrel multiplicity detector, beam, veto and T0 counters were used. The positions of the beam counters and trigger barrel detector and the target are given in Fig.1b. The carbon beam intensity was few 10^5 per the spill, the spill duration was 2-2.5 sec. The magnetic field in the center of the analyzing magnet was 0.61 T.

Monte Carlo simulation and event reconstruction

The event samples of *C+A* collisions were produced with the DCM-QGSM event generator. The passage of particles through the setup volume was simulated with the GEANT program integrated into the BmnRoot software framework. To properly describe the GEM detector response in the magnetic field the microsimulation package Garfield++ was used. The package gives very detailed description of the processes inside the GEM detector, including the drift and diffusion of released electrons in electric and magnetic fields and the electron multiplication in GEM foils, so that the output signal from the readout plane can be reproduced. To speed up the simulation the dependencies of the Lorentz shifts and the charge distributions on the readout planes on the drift distance were parameterized and used in the GEM digitization part of the BmnRoot package. The details of the detector alignment, Lorenz shift corrections are described in the paper [DeuteronPaper]. The track reconstruction method was based on a so-called “cellular automaton" approach [CBM1]. The tracks found were used to reconstruct primary and secondary vertices using the “KF-particle" formalism [CBM2]. Λ hyperons were reconstructed using their decay mode into two oppositely-charged tracks. The signal event topology (decay of a relatively long-lived particle into two tracks) defined the selection criteria: small track-to-track separation in the decay vertex, relatively large decay length of the mother particle. Since particle identification was not used in the analysis, all positive tracks were considered as protons and all negative as π^-.

Event selection criteria:

1. Number of tracks in selected events: positive>=1, negative>=1;

2. Beam halo, pile-up suppression within the readout time window: number of signals in the start detector: T0=1, number of signals in the beam counter: BC2=1, number of signals in the veto counter around the beam: Veto=0;
3. Trigger condition in the barrel multiplicity detector: number of signals BD>=2 or BD>=3 (run dependent).

The suppression factors (in %) of reconstructed events fluxes due to selection criteria 2 applied to eliminate beam halo and pile-up events in interactions of *C+C*, *C+Al*, *C+Cu* are given in Table 1.

Table 1.

Cut	1	2	3	4
T0==1	+			+
BC2==1		+		+
Veto==0			+	+
C	77.0	82.7	82.1	67.4
Al	82.4	87.5	86.0	74.0
Cu	86.0	89.1	87.9	77.9

The total suppression factors from the last column are applied to reduce the recorded beam fluxes and luminosities which are summarized in Table 2.

Table 2. Number of triggered events, beam fluxes and integrated luminosities collected in the carbon beam of 4A GeV.

Interactions, target thickness	Number of triggers / 10^6	Integrated beam flux / 10^7	Integrated luminosity / 10^{30} cm^{-2}
C+C (9 mm)	4.57	6.99	7.16
C+Al (12 mm)	5.35	4.41	3.11
C+Cu (5 mm)	5.31	4.57	1.98

Λ hyperon selection criteria:

- Number of hits in 1 Si + 6 GEM per track > 3, where hit is a combination of two strip clusters from both readout sides (*X* and *X'* views) on each detector station [GEMTDR]
- Momentum range of positive tracks: p_{pos}< 3.9 GeV/*c*
- Momentum range of negative tracks: p_{neg}> 0.3 GeV/*c*
- Distance of the closest approach of *V0* decay tracks (distance in X-Y plane between *V0* decay tracks at $Z=Z_{V0}$) : *dca* < 1 cm
- Distance between *V0* and primary vertex: *path* > 2.5 cm

Distributions of the experimental primary vertex are given in Fig.12b. Distributions of kinematical and spatial parameters used for the Λ hyperon selection are presented in Fig.12c.

Spectra of the invariant mass of (p,π^-) reconstructed in interactions of *C+C, C+Al, C+Cu* are shown in Fig.8. To extract *Λ* hyperon signal, the distributions were fitted to a combination of the Gaussian function (peak) and the 4th degree orthogonal polynomial (background) in the mass range 1.08-1.18 GeV. To avoid a bias due to possible deviation of the peak from the Gaussian shape, the numbers of *Λ* hyperons were determined not from the Gaussian fit but from the content of the background-subtracted histogram bins within ±2.5 sigma window around the peak position. Thus, the Gaussian fit was only used to better estimate the background under the peak and define the peak width. *Λ* signals in intervals of the transverse momentum p_T and rapidity y_{lab} were reconstructed using similar fit procedure, i.e. the numbers of *Λ* hyperons were calculated within ±2.5 sigma windows resulted from fits of (p,π^-) mass spectra in p_T and y intervals. The error of the *Λ* signal includes the uncertainty of the background subtraction. The statistical and systematical errors were calculated according to the formula: $sig=hist–bg$, $err(stat)=\sqrt{hist}$, $err(syst)=\sqrt{(0.5*bg)}$, assuming that the background was estimated with the uncertainty of $\sqrt{(0.5*bg)}$. If the variation of the background shape or the signal integration window gave larger uncertainties than $\sqrt{(0.5*bg)}$, the largest uncertainty was taken as a systematical error. In particular, to estimate one uncertainty of the *Λ* signal extraction, the number of *Λ* hyperons in p_T and y intervals were also calculated within the same windows as for the total *Λ* signal. If the difference in the *Λ* hyperon numbers was larger than the systematical error, this difference was taken as a systematical error.

The invariant mass spectra of (p,π^-) pairs reconstructed in *C+C, C+Al, C+Cu* interactions the p_T and y intervals are presented in Figs.2-7. The statistics of *Λ* hyperons reconstructed in *C+C, C+Al, C+Cu* interactions are summarized in Table 3 and in Fig.8.

Table 3. Reconstructed signals of *Λ* hyperons in bins of y and p_T. The first error presents the statistical uncertainty, the second error is systematical.

Target / Interval	***y***			Target / Interval	p_T		
	C	***Al***	***Cu***		***C***	***Al***	***Cu***
1.2-1.45	103±27±18	265±45±30	591±69±46	0.1-0.3	454±68±46	652±84±56	625±85±58
1.45-1.65	250±43±29	510±59±38	601±60±39	0.3-0.55	296±44±29	717±80±53	797±81±54
1.65-1.85	338±57±38	550±72±48	576±77±52	0.55-0.8	128±31±20	462±65±43	379±61±41
1.85-2.1	253±51±35	443±72±49	371±67±45	0.8-1.05	N/A	96±39±27	133±44±30

To evaluate the *Λ* hyperon acceptance and reconstruction efficiencies, minimum bias interactions of 4A GeV carbon beam with *C, Al, Cu* targets were generated with the DCM-QGSM generator. The generated particles were traced through the BM@N geometry using the GEANT simulation and reconstructed using the BmnRoot software framework. Experimental and Monte Carlo distributions of the track multiplicity, number of tracks reconstructed in the primary vertex and number of hits per track are presented in Fig.9. Distributions of the transverse momentum p_T and total momentum p of reconstructed positive and negative particles are shown in Fig.10.

To reproduce the detector effects in the reconstruction efficiency the simulated products of *Λ* hyperon decays (p,π^-) were embedded into real experimental events of *C+C, C+Al, C+Cu* interactions. Simulated amplitude signals in the Forward Silicon and GEM detectors were convoluted with amplitudes of the experimental signals in these detectors. Two-dimensional *X/Y* efficiency distributions in 6 GEM stations measured with reconstructed experimental tracks are shown in Fig.11. They were estimated using the following approach:

1. Select good quality tracks with the minimum number of hits per track *N*;
2. Check that track crosses the detector area, if yes, add one track to the denominator;
3. If there is a hit in the detector, which belongs to the track, and the number of hits on this track >*N* (i.e. track has the minimum number of hits N in the remaining detectors), add one track to the numerator;
4. Detector efficiency = sum of tracks in numerator / sum of tracks in denominator.

These efficiencies were applied to reduce the number of hits of embedded tracks of Λ decay products.

The experimental distribution of GEM hit residuals to tracks is presented in Fig.12. The corresponding distribution for embedded tracks of Λ decay products is also shown in Fig 12. The RMS of distributions are in a reasonable agreement. The invariant mass spectrum of (p,π^-) pairs reconstructed in the experimental events of *C+Cu* interactions with embedded Λ hyperon decay products is illustrated in Fig.13. The Λ signal is reproduced by a Gaussian function with the sigma of 2.4 MeV, which is consistent with the sigma of the experimental Λ distribution of 2.5 MeV. Variation of sigma of the experimental Λ and embedded Λ signal reconstructed in bins of p_T is illustrated in Fig.13b. To estimate statistical fluctuations of the experimental Λ signal, the Gaussian fit is performed for the mass distribution shifted at a half of the mass bin (1.25 MeV/c^2). The difference in sigma is presented as error bands in the plots.

The resulting Λ reconstruction efficiency is the ratio of the number of reconstructed Λ hyperons to the number of generated ones in the intervals of (p_T,y). The reconstruction efficiency can be decomposed into the following components: $\varepsilon_{rec} = \varepsilon_{acc} \cdot \varepsilon_{emb} \cdot \varepsilon_{cuts}$.. The definition of every term is given in Table 4 and their determination procedure is as follows.

Reconstructed primary vertices from experimental events were taken to serve as the interaction point for DCM-QGSM generated events with produced Λs. After the event simulation and reconstruction the successfully reconstructed Λ was counted in the numerator N_{rec} and the procedure continued with the next experimental event. In the opposite case, the current vertex was used for the next MC event. The "successful reconstruction" means that the reconstructed Λ mass was within ±5 MeV window around the table value and the reconstructed hyperon "matches" with the generated one, i.e. its momentum components are within ±0.1 and 0.15 GeV/c window from the true ones for p_x (p_y) and p_z, respectively, and rapidity within ±0.2. The detector acceptance was taken as N_{rec} / N_{gen}, where N_{gen} is the total number of MC events tried.

The accepted hyperons were used for the embedding procedure as follows. Monte Carlo digits originated from Λ decay products were added to respective (as explained above) experimental events and the reconstruction was performed again for such mixed data. This allowed us to take into account many real-life effects (GEM efficiency, zero suppression, event pile-up). Successfully reconstructed (in the explained above sense) embedded Λ gave the embedding efficiency with respect to the number of accepted ones from above.

The successfully reconstructed Λs gave the denominator for the selection efficiency calculation, i.e. efficiency of selection criteria applied for background suppression.

Table 4. Decomposition of the Λ hyperon reconstruction efficiency.

Reconstruction efficiency	$\varepsilon_{rec} = \varepsilon_{acc} \cdot \varepsilon_{emb} \cdot \varepsilon_{cuts}$
Λ geometrical acceptance in GEM detectors	$\varepsilon_{acc} = N_{acc}(y,p_T) / N_{gen}(y,p_T)$
Efficiency of reconstruction of embedded Λ	$\varepsilon_{emb} = N_{emb}(y,p_T) / N_{acc}(y,p_T)$
Efficiency of Λ selection: kinematic and spatial cuts	$\varepsilon_{cuts} = N_{rec}(y,p_T) / N_{emb}(y,p_T)$

2-dimentional (p_T,y) distributions of reconstructed Λ decay candidates in data and Monte Carlo do not perfectly agree in the shape. To adjust the Monte Carlo to the data, weights were calculated as a ratio of the normalized spectra of experimental data to the normalized spectra of simulated events: $w(y,p_T) = N_{data}(y,p_T)/N_{rec}(y,p_T)$.The 2-dimentional weights are shown in Fig.14. These weights were used to obtain 1-dimentional efficiencies according to the formula:

$$\varepsilon_{rec}(p_T) = \Sigma_y(N_{rec}(y,p_T)\cdot w(y,p_T)) / \Sigma_y(N_{gen}(y,p_T)\cdot w(y,p_T))$$
$$\varepsilon_{rec}(y) = \Sigma_{pT}(N_{rec}(y,p_T)\cdot w(y,p_T)) / \Sigma_{pT}(N_{gen}(y,p_T)\cdot w(y,p_T))$$

The actual values of efficiencies (ε_{acc}, ε_{emb}, ε_{cuts}) calculated for *C+C, C+Al, C+Cu* interactions in the y and p_T bins are shown in Figs. 16-18. The combined reconstruction efficiencies ε_{rec} calculated for *C+C, C+Al, C+Cu* interactions are presented in Fig.19.

The trigger efficiency ε_{trig} calculated for events with reconstructed Λ hyperons in interactions of carbon beam with different targets is given in Table 5. The trigger efficiency was evaluated by a convolution of the GEANT simulation of the trigger BD detector response to DCM-QGSM events with reconstructed Λ hyperons and the GEANT simulation of delta electrons produced by the carbon beam in the *C*, *Al*, *Cu* targets which were found to be the dominant source of delta electrons. The systematic errors cover the contribution of delta electrons produced in the simulated targets with the fractional thickness from 0.5 to 1 of the real targets. The trigger efficiency obtained in simulation was cross checked by the analysis of data samples with the reduced trigger requirements: BD>=1 for *C+C* interactions and BD>=2 for *C+Al* and *C+Cu* interactions. The evaluated efficiencies for events with reconstructed Λ ε(BD>=2)/ε(BD>=1,*C+C*) = 0.90, ε(BD>=3)/ε(BD>=2,*C+Al*,*C+Cu*) = 0.95 are consistent with the trigger efficiencies calculated using simulated events.

Table 5. Trigger efficiency evaluated for events with reconstructed Λ hyperons in interactions of the carbon beam with *C, Al, Cu* targets. The systematic errors take into account the uncertainty due to the delta electron background. The last row shows the trigger efficiency averaged over the data samples with trigger conditions BD>=2 and BD>=3.

Trigger / Target	***C***	***Al***	***Cu***
ε_{trig} (BD>=2)	0.906±0.010	0.955±0.010	0.904±0.01
ε_{trig} (BD>=3)		0.923±0.020	0.883±0.02

ε_{trig} (BD>=2 + BD>=3)		0.940±0.015	0.893±0.015

Distributions of the impact parameters of minimum bias interactions generated with the DCM-QGSM model are shown in Fig.26. The impact parameter distributions of generated events with Λ hyperons as well as the impact parameters of simulated events with reconstructed Λ hyperons are presented for comparison. The Λ reconstruction requirements and the trigger conditions do not change the impact parameter distributions. The ratio of the normalized impact parameter distributions for events with reconstructed Λ to events with generated Λ are shown in Fig.27. A linear fit to the ratios gives slopes which are within 0.7, 0.3, 1.5 σ consistent with zero for *C+C*, C+Al, C+Cu interactions, respectively. The mean values of the impact parameters for events with Λ hyperons generated in *C+C, C+Al, C+Cu* interactions are presented in Table 6.

Table 6. Mean impact parameters of min. bias *C+C, C+Al, C+Cu* interactions.

MC	***b*, fm (*C+C*)**	***b*, fm (*C+Al*)**	***b*, fm (*C+Cu*)**
All min bias events	3.76	4.36	5.13
Events with Λ	2.80	3.08	3.58
Events with rec. Λ	2.71	3.18	3.88

The cross section σ_Λ and yield Y_Λ of Λ hyperon production in *C+C, C+Al, C+Cu* interactions are calculated in bins of y and p_T according to the formulae:

$$\sigma_\Lambda(y,p_T)=N_{rec}^{\Lambda}(y,p_T) / (\varepsilon_{rec}(y,p_T)\cdot\varepsilon_{trig}\cdot L) \qquad Y_\Lambda(y,p_T) = \sigma_\Lambda(y,p_T) / \sigma_{inel}$$

where L is the luminosity, N_{rec}^{Λ}–the number of reconstructed Λ hyperons, ε_{rec}–the combined efficiency of the Λ hyperon reconstruction, ε_{trig}–the trigger efficiency, σ_{inel}– the cross section for minimum bias inelastic *C+A* interactions. The cross section for inelastic C+C interactions is taken from the measurement [AngelovCC]. The cross sections for inelastic *C+Al*, *C+Cu* interactions are taken from the predictions of the DCM-QGSM model which are consistent with the results calculated by the formula: $\sigma_{inel} = \pi R_0^2 (A_P^{1/3} + A_T^{1/3})^2$, where R_0 = 1.2 fm is an effective nucleon radius, A_P and A_T are atomic numbers of the beam and target nucleus [HadesL0]. The uncertainties for *C+Al, C+Cu* inelastic cross sections are estimated by using the alternative formula: $\sigma_{inel} = \pi R_0^2 (A_P^{1/3} + A_T^{1/3} - b)^2$ with R_0 = 1.46 fm and b = 1.21 [AngelovCC].

Table 7.

Interaction	***C+C***	***C+Al***	***C+Cu***
Inelastic cross section, mb	830±50	1260±50	1790±50

The yields of Λ hyperons in minimum bias *C+C, C+Al, C+Cu* interactions are measured in the kinematic range on the Λ transverse momentum of $0.1<p_T<1.0$ GeV/*c* and the Λ rapidity in the laboratory frame of $1.2<y_{lab}<2.1$. Due to lack of the significant signal above the background at $p_T>0.75$ GeV/*c* in *C+C* interactions, the measured p_T range was limited to $0.1<p_T<0.75$ GeV/*c*. The rapidity of the beam-target nucleon-nucleon CM system calculated for an interaction of the beam with $\boldsymbol{T_0}$=4 GeV/nucleon with a fixed target is y_{CM}=1.17. The transformation of the y

distribution to c.m.s. gives $y^*=y_{lab}-y_{CM}$. The differential spectra of the Λ yields in y_{lab} are measured in the Λ transverse momentum range of $0.1<p_T<.05$ GeV/c for *C+C, C+Al, C+Cu*. The differential spectra of the Λ yields in p_T are measured in the Λ rapidity range of $1.2<y_{lab}<2.1$. The p_T and *y* spectra are presented in Figs. 20-22 for *C+C, C+Al, C+Cu* interactions, respectively. The predictions of the DCM-QGSM and URQMD models are shown for comparison. In Fig.23 the measured spectra of the Λ yields in p_T are parameterized by the form: $1/p_T \cdot d^2N/dp_Tdy=N\cdot exp(-(m_T-m_\Lambda)/T)$, where $m_T=\sqrt{(m_\Lambda^2+p_T^2)}$ is the transverse mass, the normalization *N* and temperature *T* are free parameters of the fit. The experimental Λ spectra are compared with the predictions of the DCM-QGSM and URQMD models. The parametrization of the DCM-QGSM and URQMD spectra are shown in Fig.24. The values of the temperature T_0, extracted from the fit of the p_T spectra, are summarized in Table 8.

Table 8.Temperature parameter extracted from the fit of the p_T spectra.

	T_0, MeV (*C+C*)	**T_0, MeV (*C+Al*)**	**T_0, MeV (*C+Cu*)**
Experiment χ^2 / ndf	$98 \pm 24 \pm 25$ 2.04/1	$157 \pm 24 \pm 12$ 2.51/2	$160 \pm 27 \pm 21$ 0.39/2
DCM-QGSM	122	129	131
UrQMD	107	127	132

The systematic error of the Λ yield in every p_T and *y* bin is calculated via a quadratic sum of uncertainties coming from the following sources:

- Systematic errors of the embedding efficiency estimated by embedding the Λ decay products into data samples collected in different run periods.

Table 9. Systematic uncertainty of the embedding efficiency.

Target / Interval	***y***			Target / Interval	***p_T***		
	***C*, sys%**	***Al*, sys%**	***Cu*, sys%**		***C*, sys%**	***Al*, sys%**	***Cu*, sys%**
1.2-1.45	2.09	4.22	2.93	0.1-0.3	4.94	9.37	6.61
1.45-1.65	1.75	4.11	3.31	0.3-0.55	3.07	0.64	1.30
1.65-1.85	7.96	4.78	4.19	0.55-0.8	4.59	0.34	0.08
1.85-2.1	5.44	1.24	6.09	0.8-1.05	3.03	6.28	2.36

- Systematic errors estimated by two methods of re-weighting the Monte Carlo (y,p_T) distribution to adjust it to the measured (y,p_T) distribution: 1) using 2-dimentional weight $w(y,p_T)$ in the measured (y,p_T) bin; 2) using product of 1-dimentional weights calculated as $w(p_T)\cdot w(y)$.
- The Λ yield normalization uncertainty calculated as a quadratic sum of uncertainties of the trigger efficiency and inelastic cross section.

The systematic uncertainties are summarized in Tables 10 and 11.

Table 10.Systematic uncertainty of the total reconstruction efficiency.

Target / Interval	***y***			Target / Interval	***p_T***		
	***C*, sys%**	***Al*, sys%**	***Cu*, sys%**		***C*, sys%**	***Al*, sys%**	***Cu*, sys%**
1.2-1.45	7.39	8.50	6.57	0.1-0.3	8.70	8.20	5.85
1.45-1.65	7.80	6.39	3.40	0.3-0.55	7.14	6.05	5.21

1.65-1.85	9.08	7.60	4.26	0.55-0.8	11.23	10.48	3.19
1.85-2.1	7.34	7.35	5.01	0.8-1.05	2.06	7.16	2.32

Table 11. Total systematic uncertainty.

Target / Interval	***y***			Target / Interval	***p_T***		
	C, sys%	***Al***, sys%	***Cu***, sys%		***C***, sys%	***Al***, sys%	***Cu***, sys%
1.2-1.45	19.0	14.8	10.5	0.1-0.3	14.2	15.1	12.7
1.45-1.65	14.1	10.6	8.0	0.3-0.55	10.7	9.6	8.6
1.65-1.85	16.5	12.5	10.8	0.55-0.8	19.8	14.0	11.3
1.85-2.1	16.6	13.3	14.4	0.8-1.05	N/A	29.7	22.7
Normalization	6.0	4.0	2.8	Normalization	6.0	4.0	2.8

The integrated yields of Λ hyperons produced in the kinematic range of $0.1<p_T<1.05$ GeV/*c* and $1.2<y_{lab}<2.1$ in minimum bias *C+C, Al, Cu* interactions are summarized in Table 12. To extrapolate the measured yields to the full kinematic range the predictions of the DCM-QGSM and URQMD models are used. The model extrapolation factors and the estimated yields and cross sections of the Λ hyperon production in *C+C, C+Al, C+Cu* minimum bias interactions are given in Table 12.

Table 12. Extrapolation factors to the full kinematical range, yields and cross sections.

	C	***Al***	***Cu***
DCM-QGSM URQMD extrapolation factors	6574/2474 1827/639	10539/3413 3248/1056	15817/3545 5509/1360
Yields in the measured kin range $0.1<p_T<1.05$ GeV/c, $1.2<y_{lab}<2.1$	0.0214±0.0023±0.0024	0.0431±0.0034±0.0035	0.0561±0.0039±0.0047
Yields in the full kinematic range N part DCM-QGSM	0.0589±0.0063±0.0065 9	0.133±0.010±0.011 13.4	0.239±0.017±0.020 23
Λ cross section in min. bias interactions, mb	48.9 ± 5.2 ± 5.1	167 ± 13 ± 13	427 ± 30 ± 29

The Λ yields and production cross sections in *C+C* interactions can be compared with the previous results of 23.2±2.5 mb [ArmutCC] and 24±6 mb [ArakelianCC] measured in interactions of the carbon beam with the momentum of 4.2 GeV/*c* per nucleon (beam kinetic energy of 3.36 GeV per nucleon) with the Propane Chamber experiment, as well as with the result of the HADES experiment at 2A GeV. In Fig.25 the BM@N result for Λ yield is compared with the results taken from [ArakelianCC], [ArmutCC], [HadesL0]. The predictions of the DCM-QGSM and UrQMD models are also shown for comparison.

Table 13. Yields and cross sections of Λ hyperon production in interactions of light and medium nucleus.

Interacting nucleus /	Beam momentum,	Λ cross section, mb	Λ yield, $\cdot 10^{-2}$

reference	kinetic energy (T_0)		
He_4+Li_6	4.5 GeV/c (3.66A GeV)	5.9± 1.5	1.85 ± 0.5
C+C	4.2 GeV/c (3.36A GeV)	24 ± 4	2.89±0.72
C+C, propane Chamber	4.2 GeV/c (3.36A GeV)	23.2±2.5	2.8 ± 0.3
p+p	4.95 GeV/c (4.1 GeV)		2.3 ± 0.4
C+C, HADES	2A GeV	$8.7\pm1.1\pm^{3.2}_{1.6}$	$0.92\pm0.12\pm^{0.34}_{0.17}$
Ar+KCl, HADES	1.76A GeV		3.93±0.14±0.15
Ar+KCl, FOPI	1.93A GeV		3.9±0.14±0.08
Ni+Ni, FOPI, central 390 mb from 3.1 *b*	1.93A GeV		$0.137\pm0.005\pm^{0.009}_{0.025}$
Ni+Cu, EOS, full *b*<8.9 fm / central *b*<2.4 fm	2A GeV	112±24 / 20±3	
Ar+KCl, central *b*<2.4 fm	1.8A GeV	7.6±2.2	

To compare yields of particle production in nucleus-nucleus interactions, they are usually normalized to the mean number of nucleons participating in interactions (Participants). The numbers of Participants in minimum bias *C+C, C+Al, C+Cu* interactions are estimated using the DCM-QGSM model [GenisPart]. The results (*A1+A2*) are shown in Table 14.

Table 14. Number of Participants in minimum bias *A+A* events at 4A GeV.

A_1A_2	A_1	A_2	$A_1 + A_2$
CC	4.5	4.5	9.0
CAl	5.23	8.14	13.37
CCu	6.21	16.79	23.0

Bibliography

[DeuteronPaper] D.Baranov et al., First Results from BM@N Technical Run with Deuteron Beam, Phys. Part. Nucl. Lett. 15, no. 2, 148 (2018)

[GEMTDR] http://bmnshift.jinr.ru/wiki/lib/exe/fetch.php?media=tdr_gem_may2017_v1.doc

[CBM1] V. Akishina and I. Kisel. Time-based cellular automaton track finder for the CBM experiment - 2015. J. Phys.: Conf. Ser. 599, 012024

[CBM2] S. Gorbunov and I. Kisel. Reconstruction of decayed particles based on the Kalman filter - 2007. CBM-SOFTnote--003

[GenisPart] Result of Genis Musulmanbekov, private communication

[AnikinaCC] N.Anikina et al., Z.Phys.C, 25,(1984),1

[ArmutCC] D.Armutlijsky et al., P1-85-220, JINR, Dubna

[ArakelianCC] S.Arakelian et al., P1-83-354, JINR, Dubna

[AngelovCC] H.Angelov et al., P1-80-473, JINR, Dubna

[HadesL0] Kalliopi Kanaki, PhD “Study of Λ hyperon production in *C+C* collisions at 2A GeV beam energy with the HADES spectrometer”, 2007

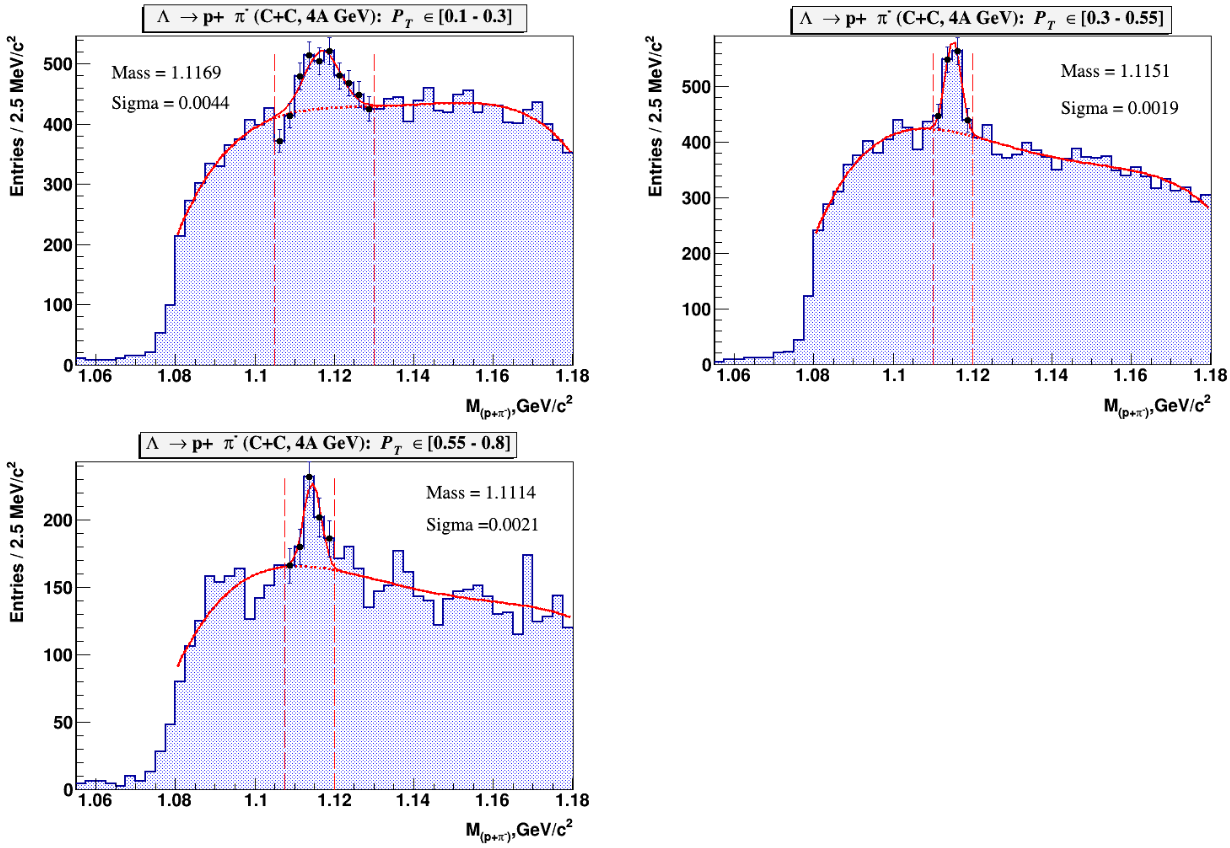

Fig. 2. $\Lambda \rightarrow p\pi^-$ signal reconstructed in $C+C$ interactions in bins of the transverse momentum p_T. The signal is fitted by a Gaussian function, the background is fitted by the 4th degree orthogonal polynomial. The vertical dashed lines indicate the mass range of ±2.5 sigma of the total Λ signal reconstructed in $C+C$ interactions.

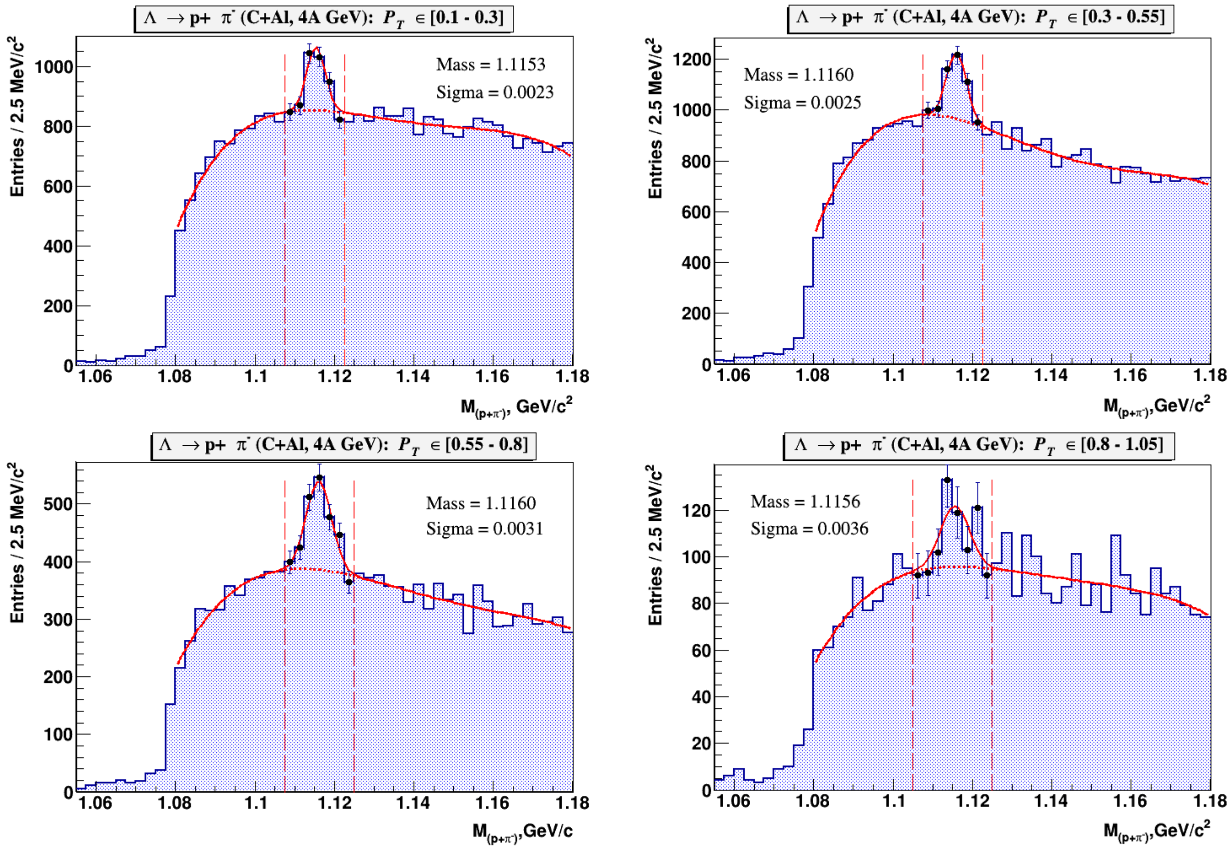

Fig. 3. $\Lambda \rightarrow p\pi^-$ signal reconstructed in *C+Al* interactions in bins of the transverse momentum p_T. The signal is fitted by a Gaussian function, the background is fitted by the 4th degree orthogonal polynomial. The vertical dashed lines indicate the mass range of ±2.5 sigma of the total Λ signal reconstructed in *C+Al* interactions.

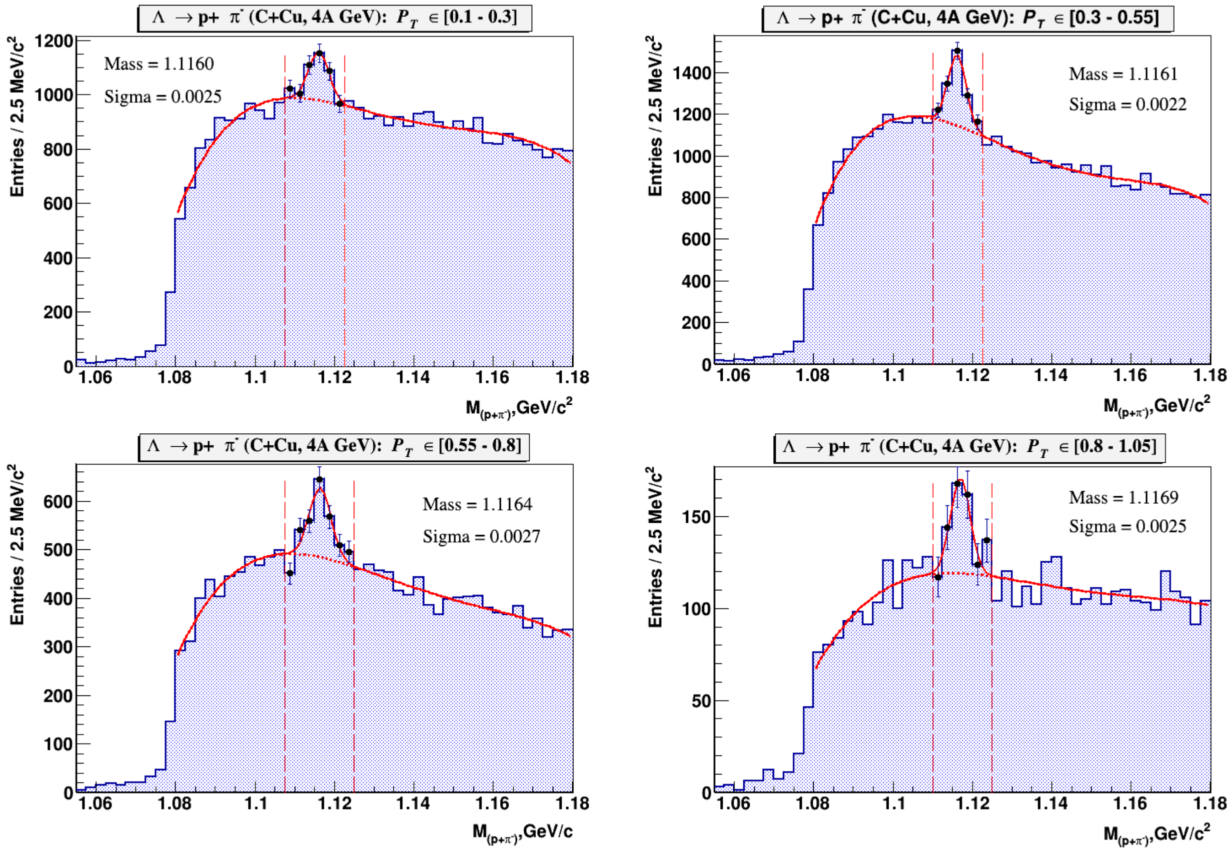

Fig. 4. $\Lambda \rightarrow p\pi^-$ signal reconstructed in *C+Cu* interactions in bins of the transverse momentum p_T. The signal is fitted by a Gaussian function, the background is fitted by the 4th degree orthogonal polynomial. The vertical dashed lines indicate the mass range of ±2.5 sigma of the total Λ signal reconstructed in *C+Cu* interactions.

276

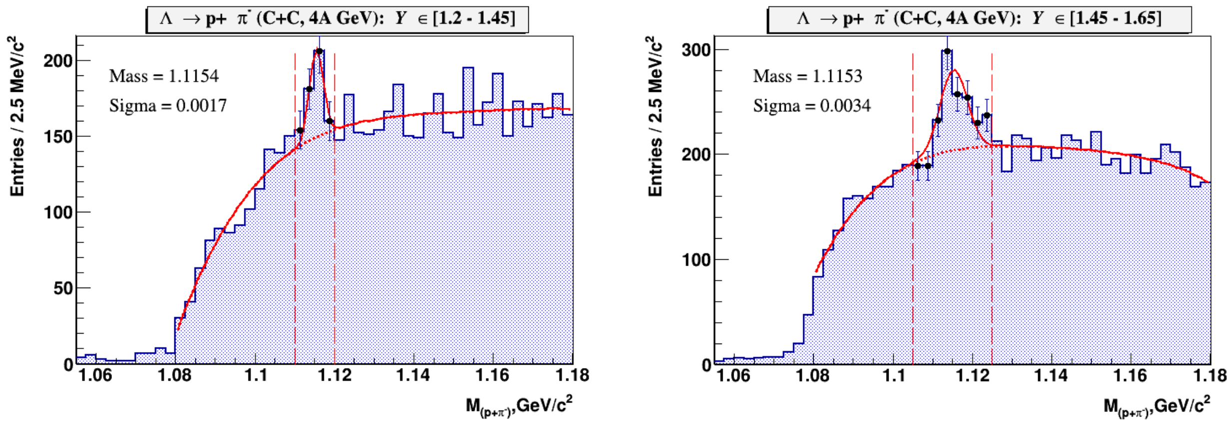

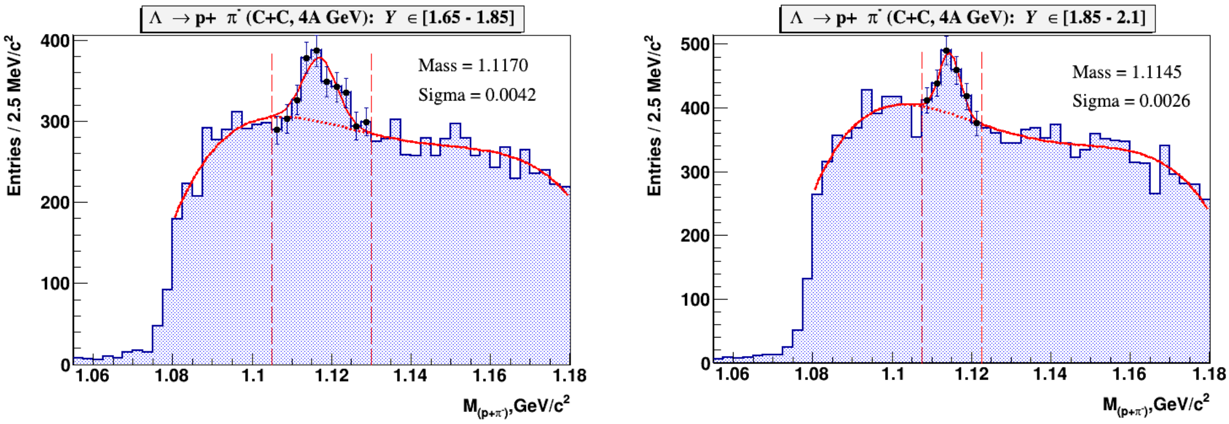

Fig. 5. $\Lambda \rightarrow p\pi^-$ signal reconstructed in *C+C* interactions in bins of the rapidity *y*. The signal is fitted by the Gaussian function, the background is fitted by the 4th degree orthogonal polynomial. The vertical dashed lines indicate the mass range of ±2.5 sigma of the total *Λ* signal reconstructed in *C+C* interactions.

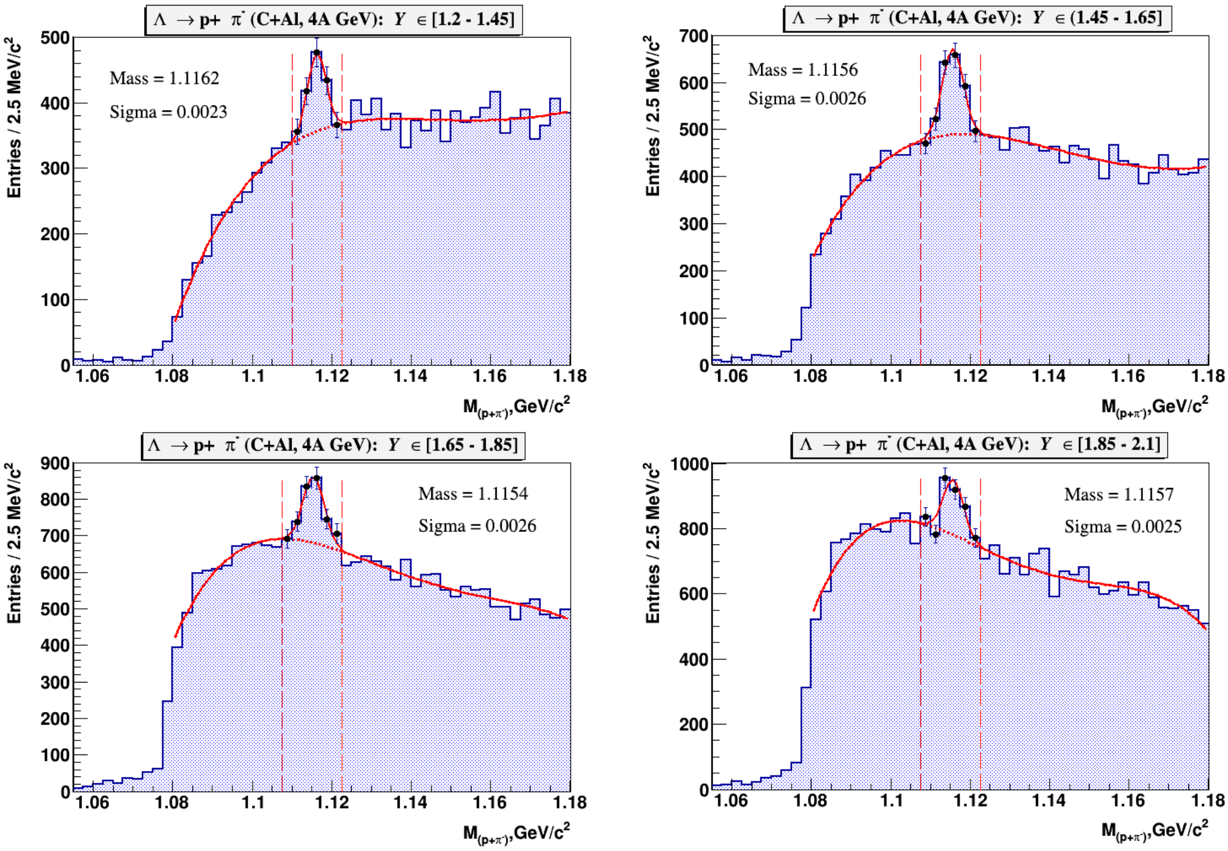

Fig. 6. $\Lambda \rightarrow p\pi^-$ signal reconstructed in *C+Al* interactions in bins of the rapidity *y*. The signal is fitted by the Gaussian function, the background is fitted by the 4th degree orthogonal polynomial. The vertical dashed lines indicate the mass range of ±2.5 sigma of the total *Λ* signal reconstructed in *C+Al* interactions.

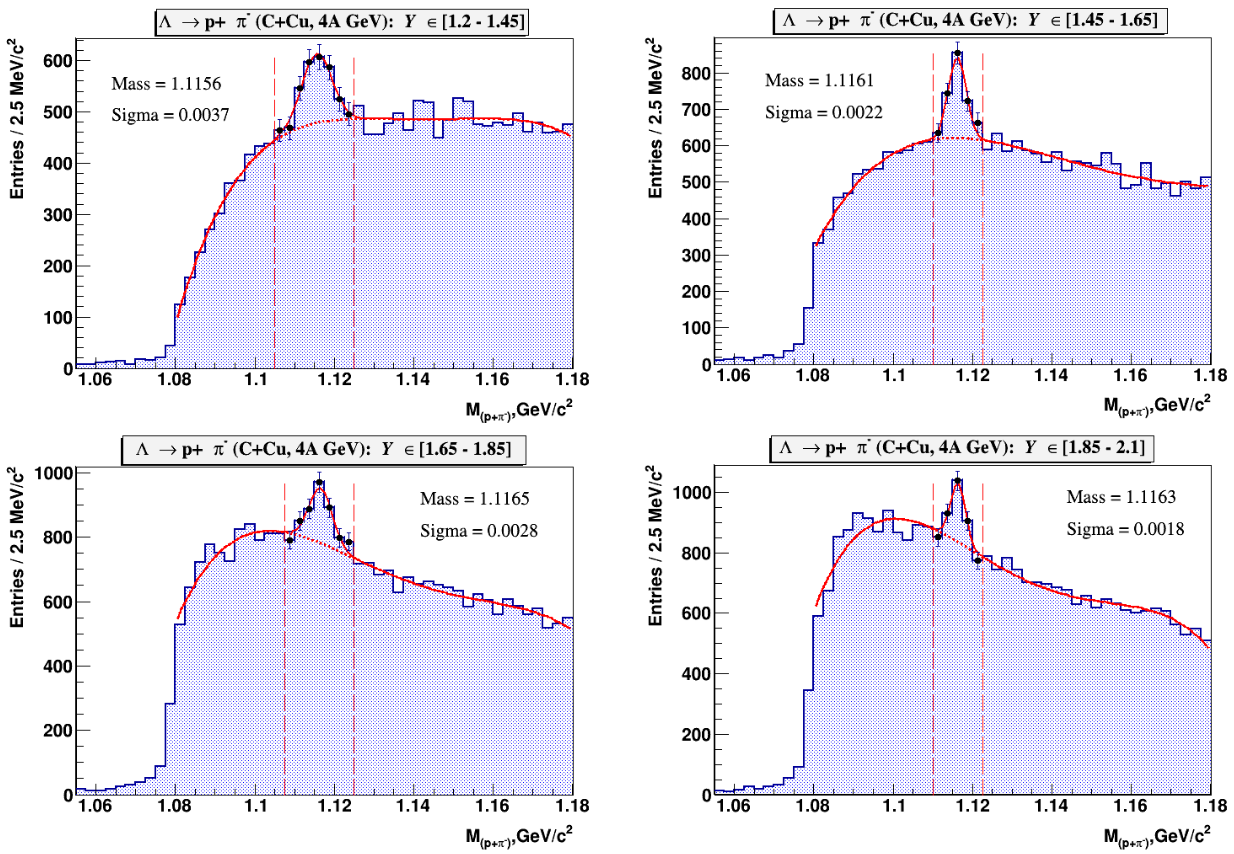

Fig. 7. $\Lambda \rightarrow p\pi^-$ signal reconstructed in *C+Cu* interactions in bins of the rapidity *y*. The signal is fitted by the Gaussian function, the background is fitted by the 4th degree orthogonal polynomial. The vertical dashed lines indicate the mass range of ±2.5 sigma of the total Λ signal reconstructed in *C+Cu* interactions.

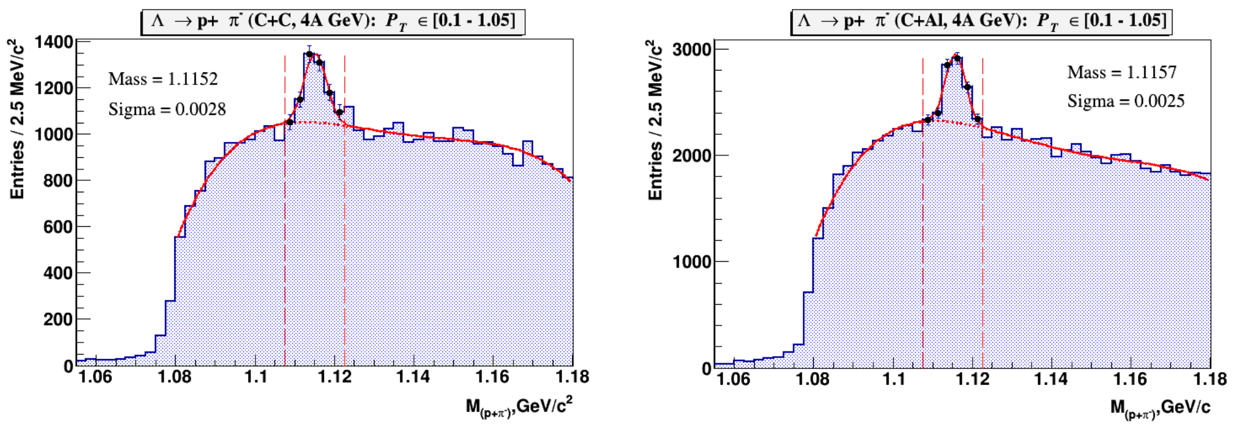

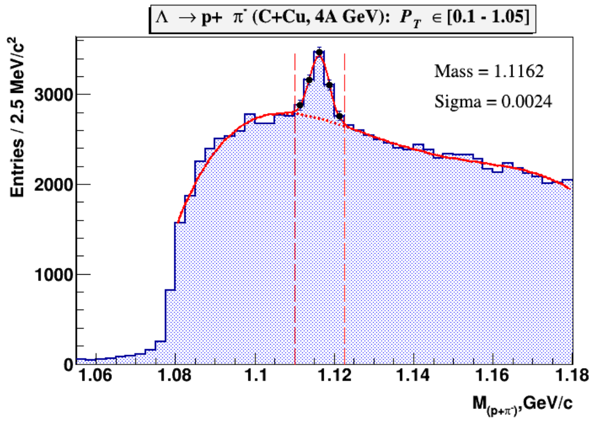

Fig. 8. $\Lambda\to p\pi^-$ signal reconstructed in interactions of the carbon beam with targets: *C, Al, Cu.* The signal is fitted by the Gaussian function, the background is fitted by the 4th degree orthogonal polynomial.

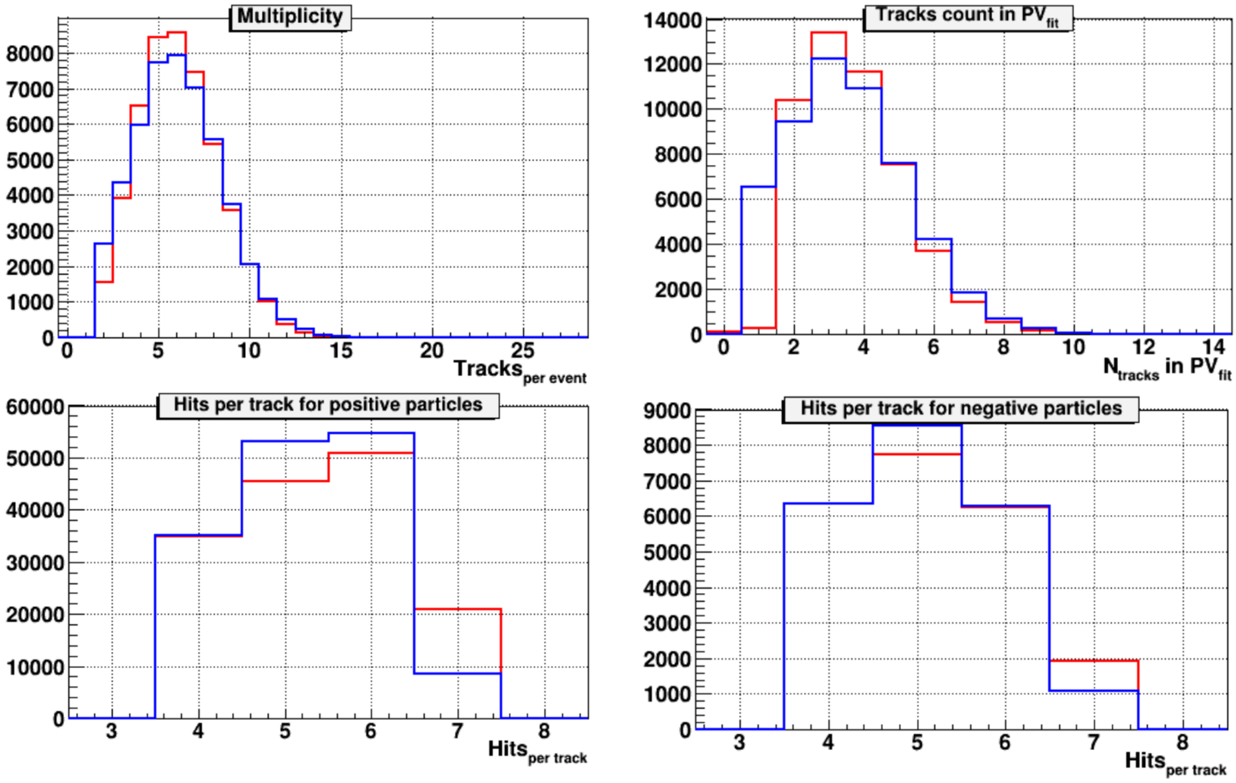

Fig.9. *C+Cu* interactions: comparison of experimental distributions (red lines) and Monte Carlo GEANT distributions of events generated with the DCM-QGSM model (blue lines): track multiplicity per event; number of tracks reconstructed in the primary vertex; number of hits per positive particle reconstructed in 1 Si + 6 GEM detectors; number of hits per negative particle.

281

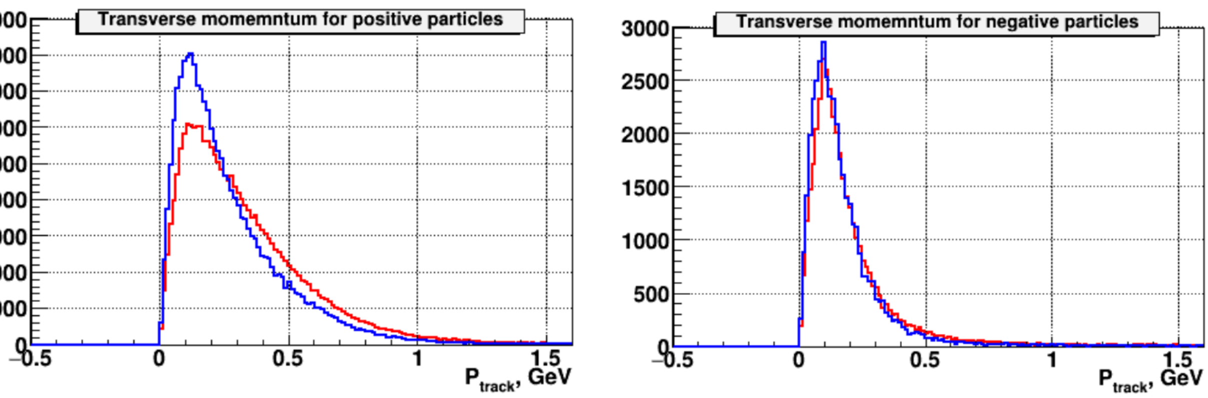

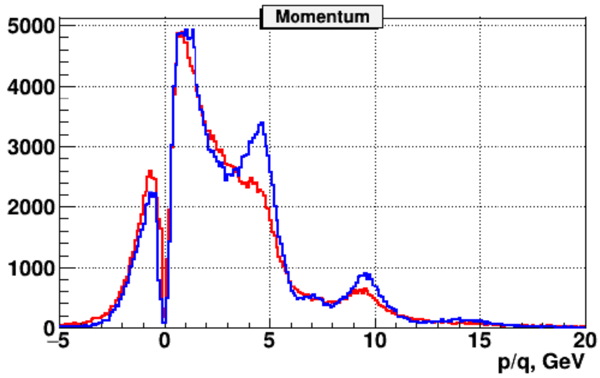

Fig. 10. $C+Cu$ interactions: comparison of experimental data (red curves) and DCM-QGSM + GEANT Monte Carlo simulation (blue curves): transverse momentum of positive particles; transverse momentum of negative particles; total momentum of negative (p/q<0) and positive particles (p/q>0).

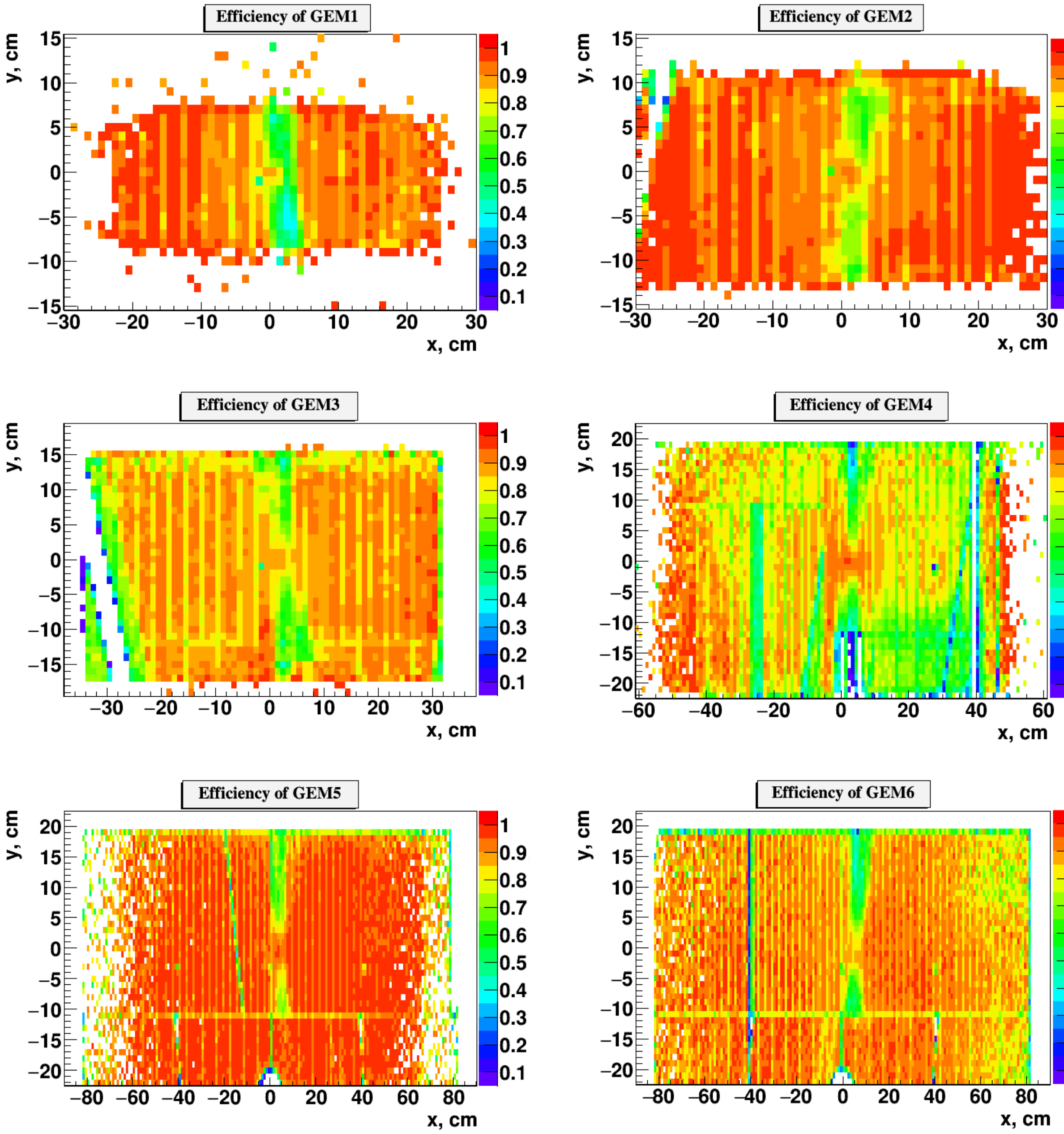

Fig. 11. Two-dimensional *X/Y* efficiency distributions in 6 GEM stations measured with

experimental tracks and implemented into Monte Carlo simulation.

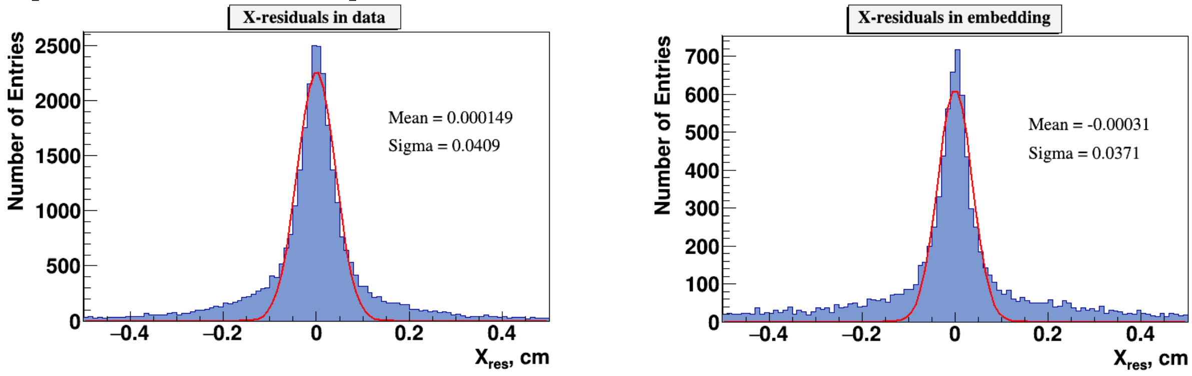

Fig. 12. Residual distributions of GEM hits with respect to reconstructed tracks: left) experimental data, right) reconstructed tracks of embedded *Λ* decay products.

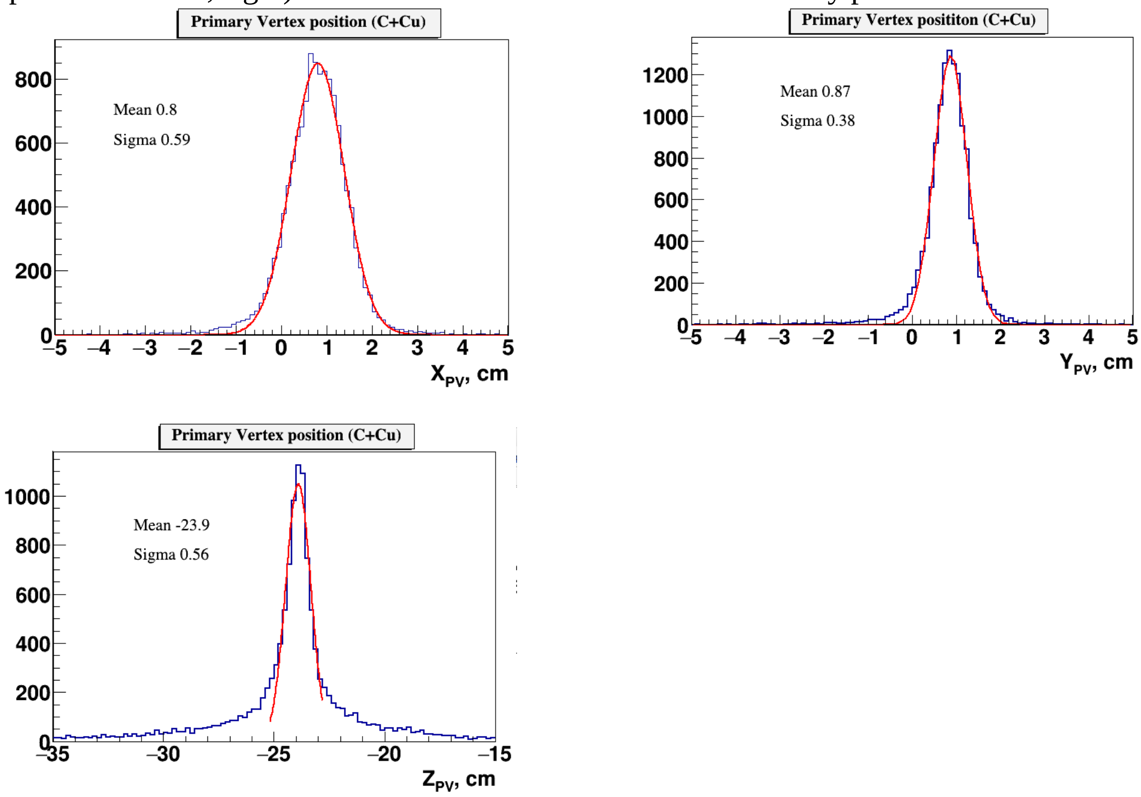

Fig. 12b. *X*,*Y*,*Z* distributions of the experimental primary vertex.

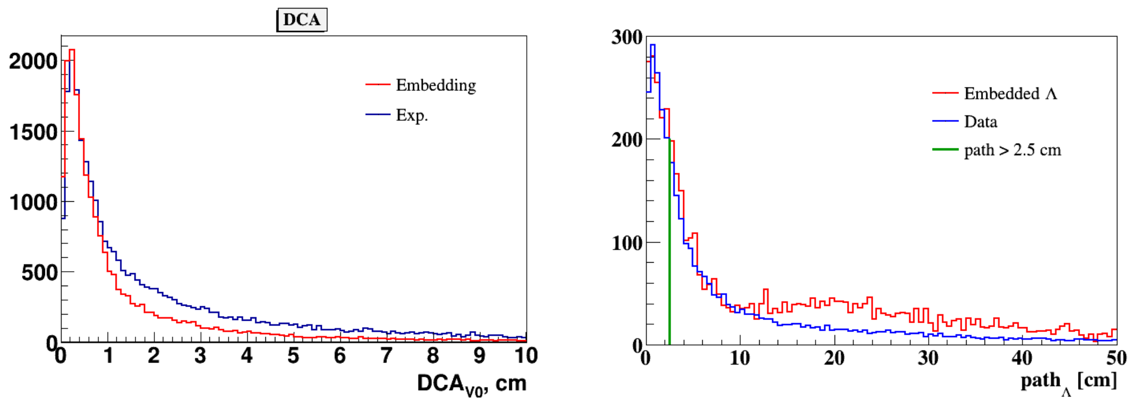

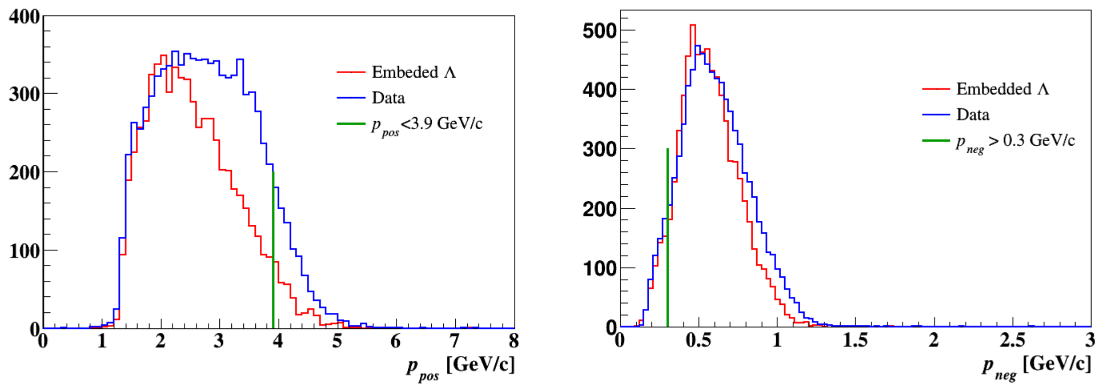

Fig.12c. Distance of the closest approach of *V0* decay tracks (DCA), distance between the primary vertex and *V0* (path), momentum distributions of positive, negative tracks from *V0* decays. Experimental data are compared with distributions for embedded *Λ* hyperons.

283

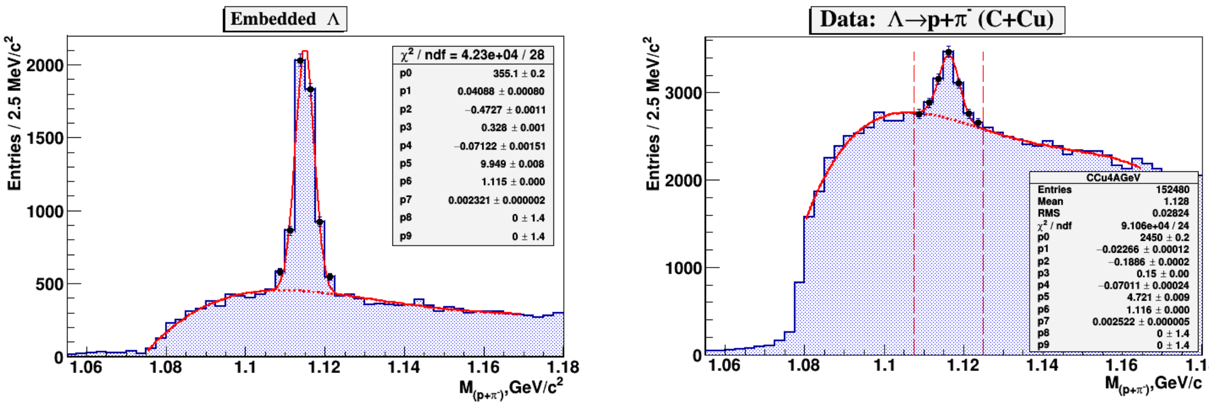

Fig. 13. The invariant mass spectrum of (p,π^-) pairs reconstructed in the experimental events of *C+Cu* interactions with embedded *Λ* hyperon decay products (left); The invariant mass spectrum of (p,π^-) pairs reconstructed in *C+Cu* interactions (right).

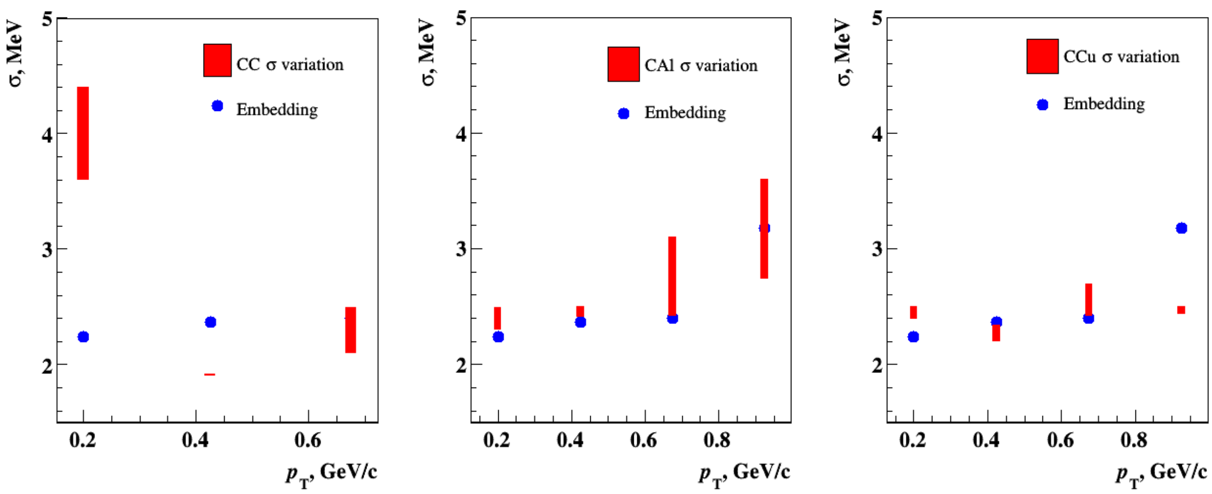

Fig.13a. Variation of sigma of the experimental *Λ* and embedded *Λ* signals reconstructed in bins of p_T in *C+C, C+Al, C+Cu* interactions. To estimate statistical fluctuations of the experimental *Λ* signal, the Gaussian fit is performed for the mass distribution shifted at a half of the mass bin (1.25 MeV/c^2). The differences in sigma are presented as error bands.

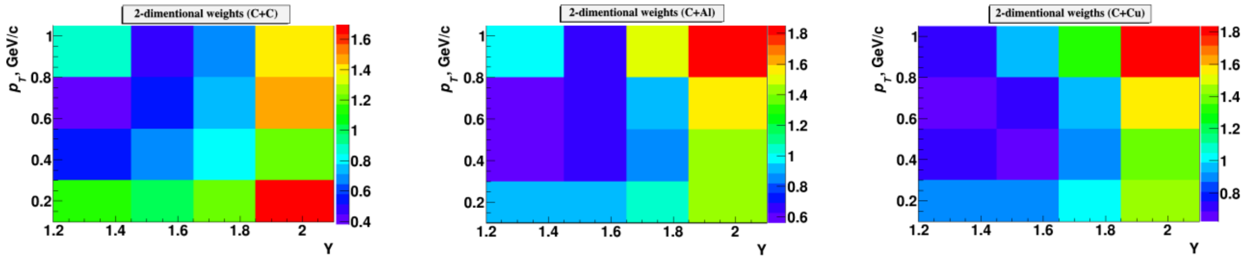

Fig. 14. 2-dimentional weights $w(y,p_T)$ obtained as a ratio of the numbers of Λ candidates in the data and simulated events for *C+C, C+Al, C+Cu* interactions.

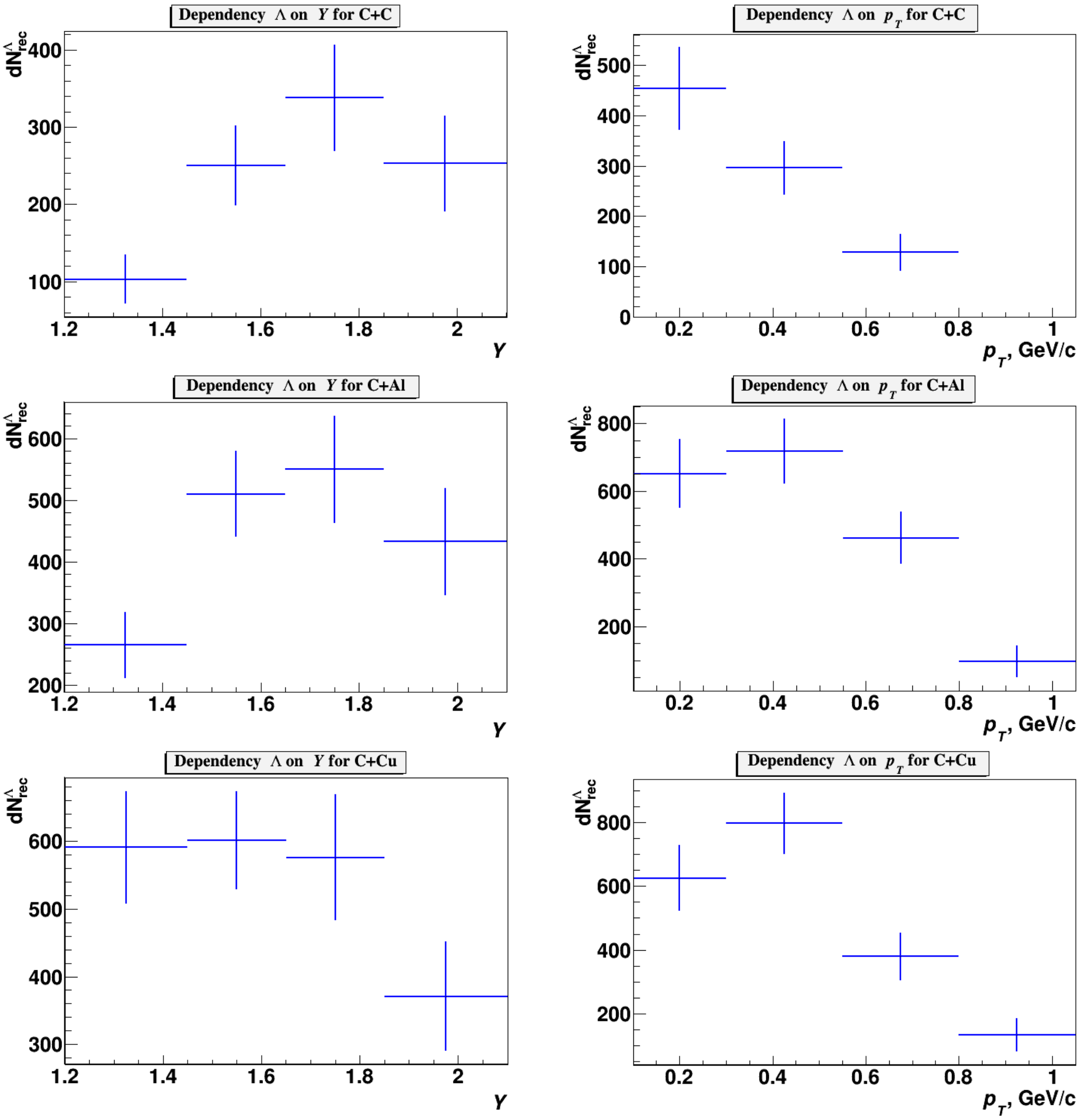

Fig.15. Number of reconstructed Λ hyperons in *C+C, C+Al, C+Cu* data samples in bins of y and p_T.

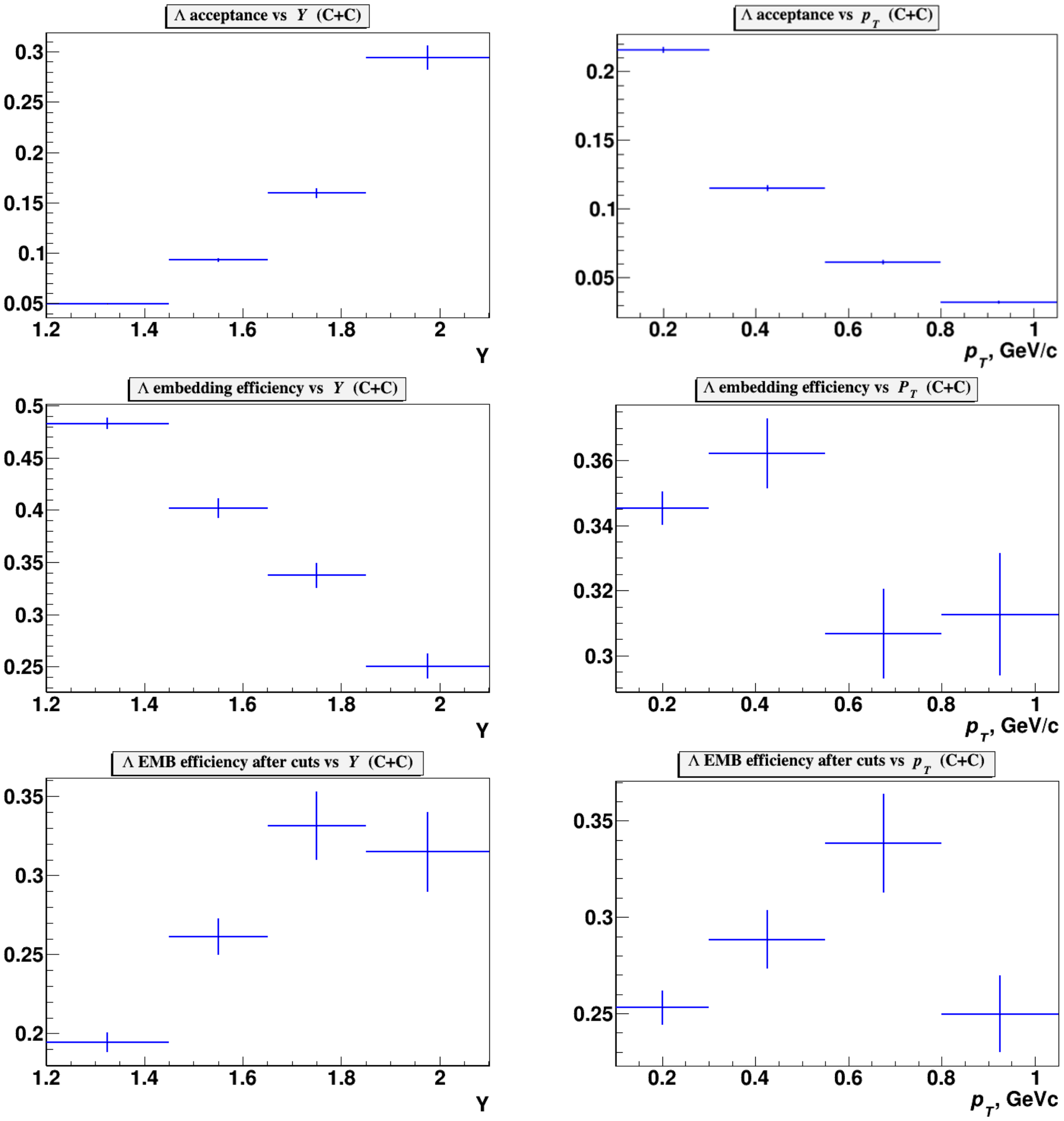

Fig.16. *Λ* geometrical acceptance (ε_{acc}); efficiency of reconstruction of embedded *Λ* (ε_{emb}); efficiency of kinematical and spatial cuts applied for *Λ* reconstruction (ε_{cuts}) as functions of rapidity *y* (left plots) and p_T (right plots). Results are shown for *C*+*C* interactions.

286

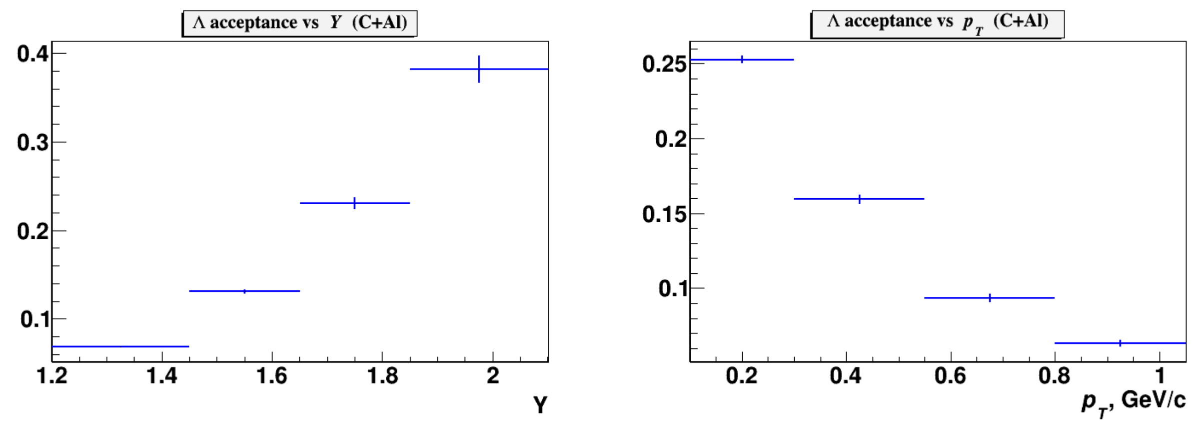

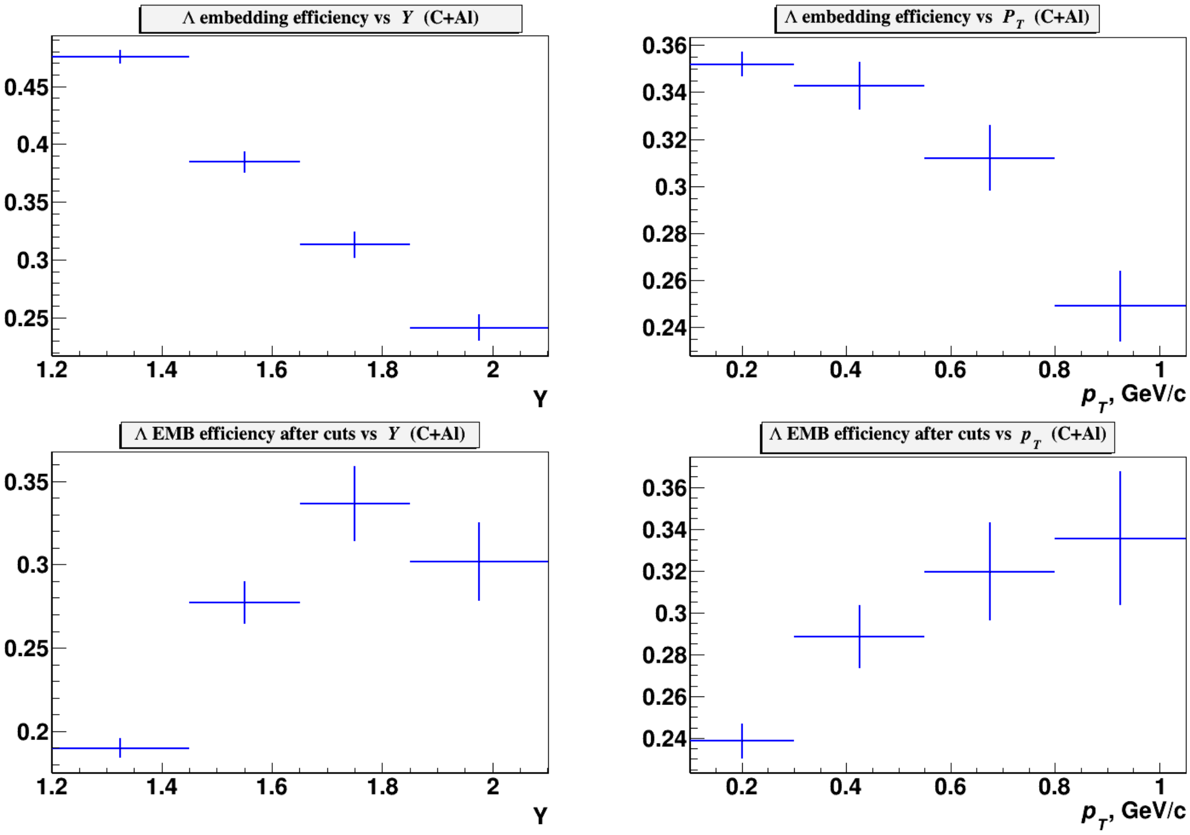

Fig.17. Λ geometrical acceptance (ε_{acc}); efficiency of reconstruction of embedded Λ (ε_{emb}); efficiency of kinematical and spatial cuts applied for Λ reconstruction (ε_{cuts}) as functions of rapidity y (left plots) and p_T (right plots). Results are shown for $C+Al$ interactions.

287

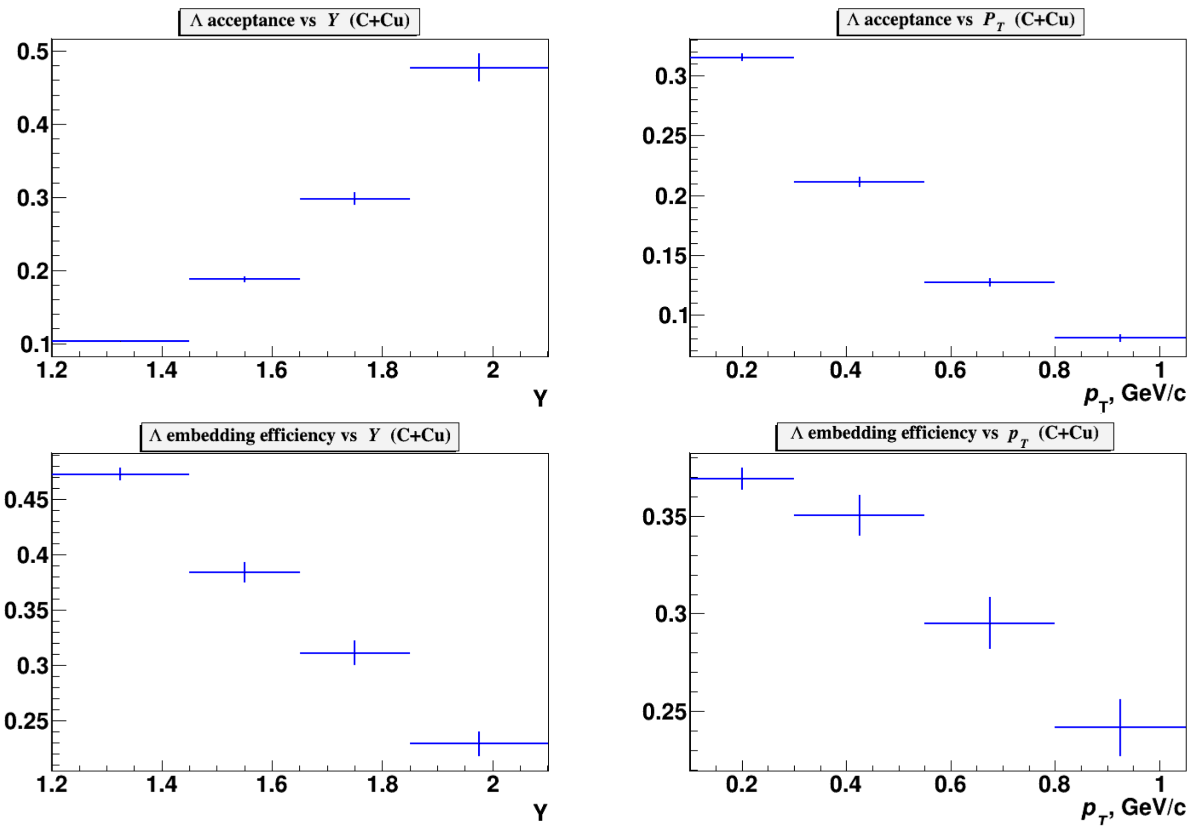

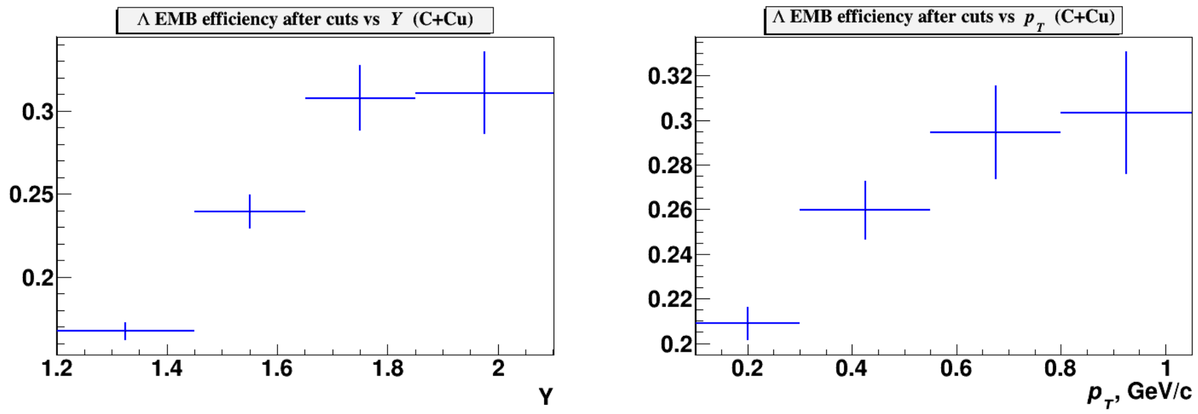

Fig.18. Λ geometrical acceptance (ε_{acc}); efficiency of reconstruction of embedded Λ (ε_{emb}); efficiency of kinematical and spatial cuts applied for Λ reconstruction (ε_{cuts}) as functions of rapidity y (left plots) and p_T (right plots). Results are shown for $C+Cu$ interactions.

288

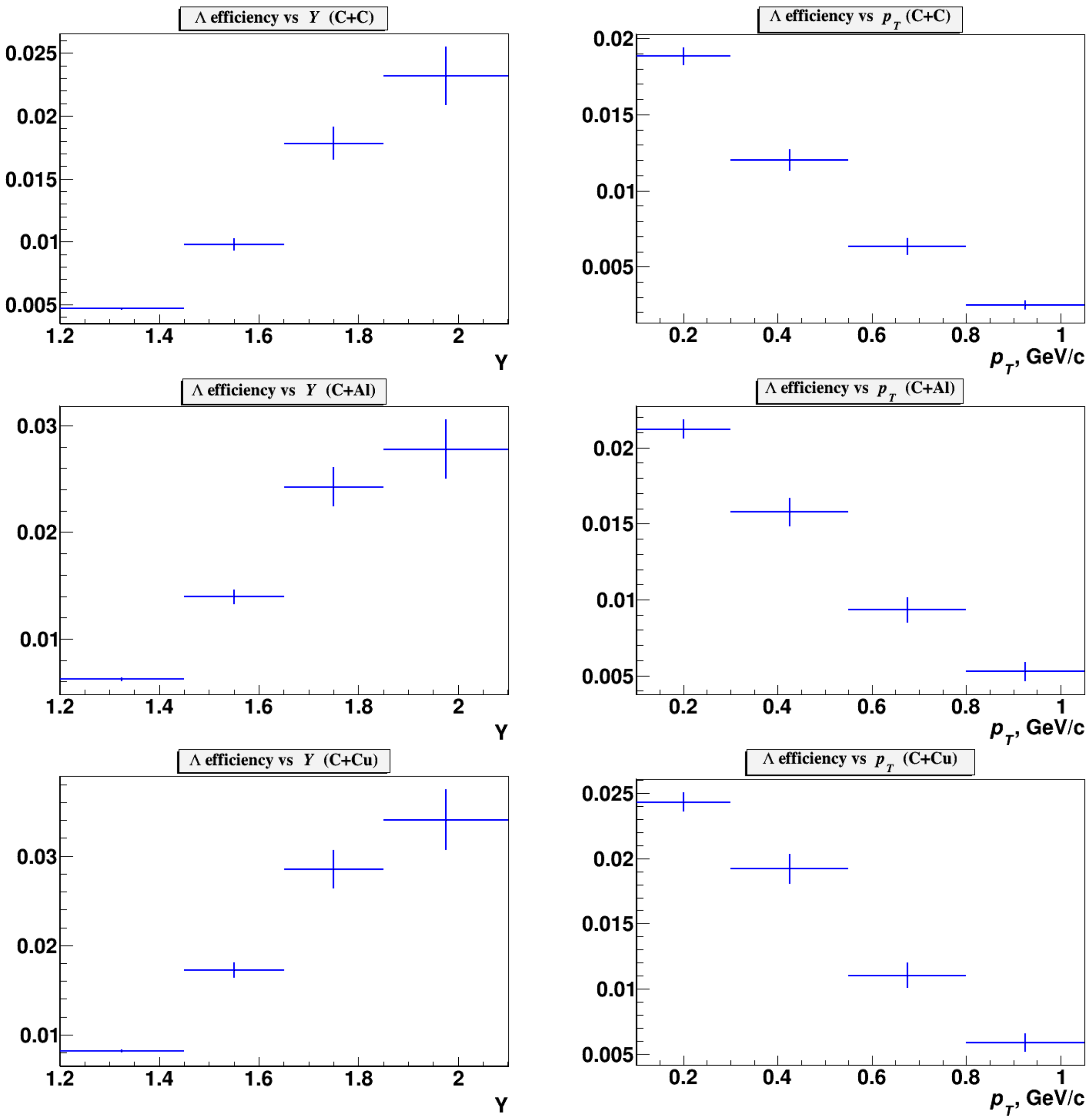

Fig.19. Combined efficiency of Λ reconstruction (ε_{acc} , ε_{emb} , ε_{cuts}) in the y and p_T bins evaluated for $C+C$ interactions (upper plots), $C+Al$ interactions (middle plots) and $C+Cu$ interactions (lower plots).

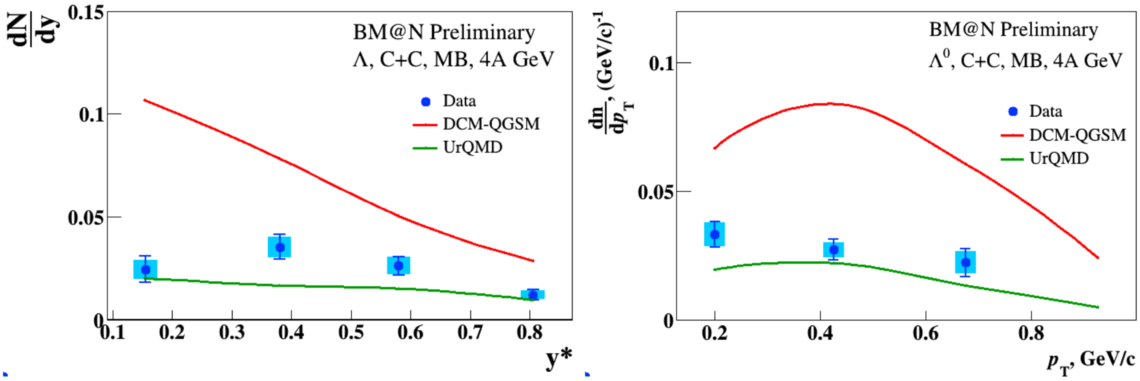

Fig. 20. Reconstructed yields (multiplicities) of *Λ* hyperons in minimum bias *C+C* interactions vs rapidity *y** in c.m.s. and transverse momentum p_T (blue crosses). Predictions of the DCM-QGSM and UrQMD models are shown as red and green lines.

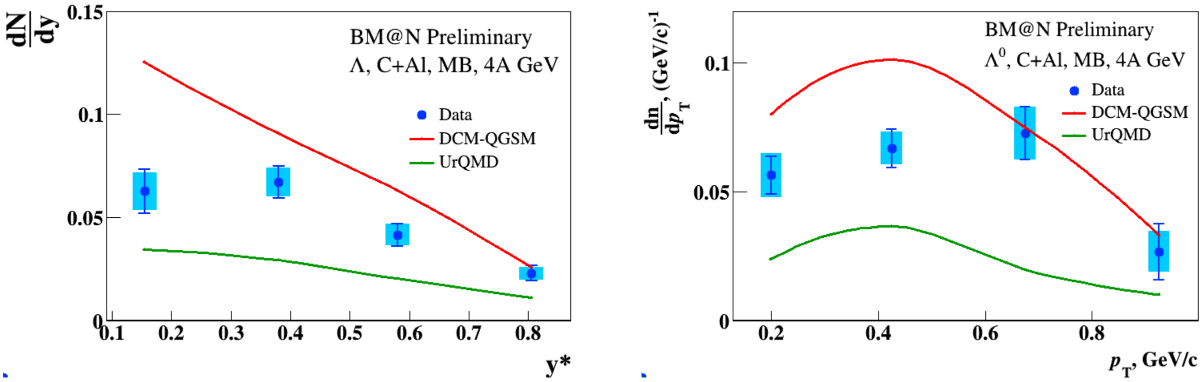

Fig. 21. Reconstructed yields (multiplicities) of *Λ* hyperons in minimum bias *C+Al* interactions vs rapidity *y** in cm.s. and transverse momentum p_T (blue crosses). Predictions of the DCM-QGSM and UrQMD models are shown as red and green lines.

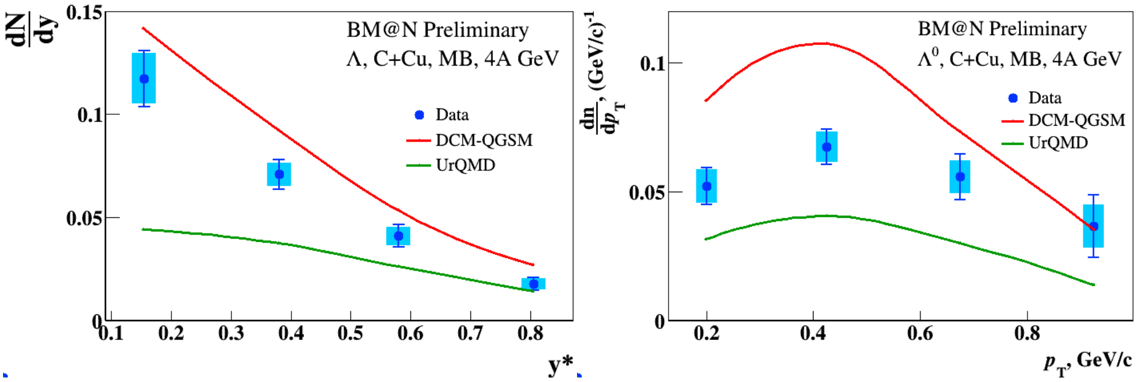

Fig. 22. Reconstructed yields (multiplicities) of *Λ* hyperons in minimum bias *C+Cu* interactions vs rapidity *y** in c.m.s. and transverse momentum p_T (blue crosses). Predictions of the DCM-QGSM and UrQMD models are shown as red and green lines.

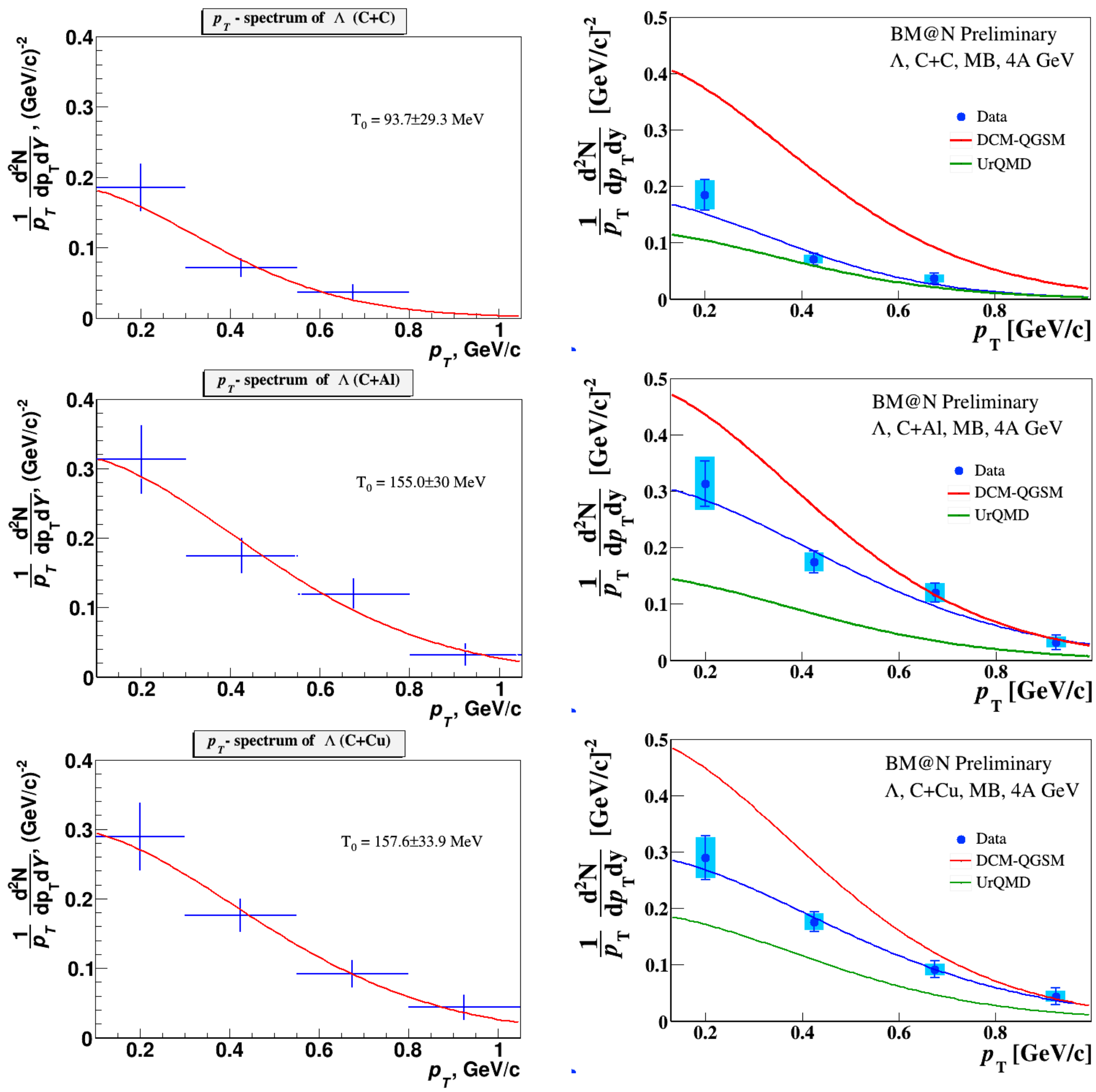

Fig. 23. Right plot) Efficiency-corrected reconstructed p_T spectra of Λ hyperon yields (multiplicities) in minimum bias $C+C$, $C+Al$, $C+Cu$ interactions (blue crosses). Predictions of the DCM-QGSM and URQMD models are shown as red and green lines, respectively. Left plot) Thermal fit results with the inverse slope parameter T_0.

291

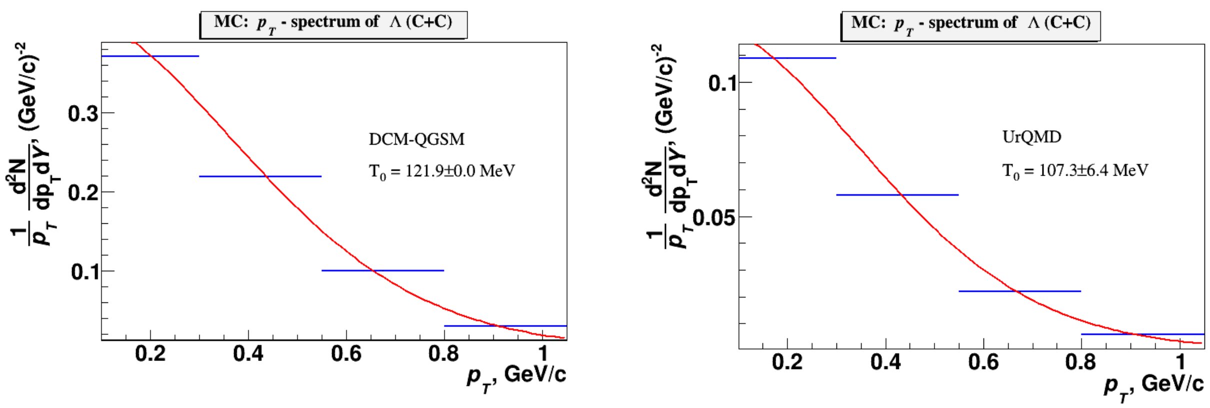

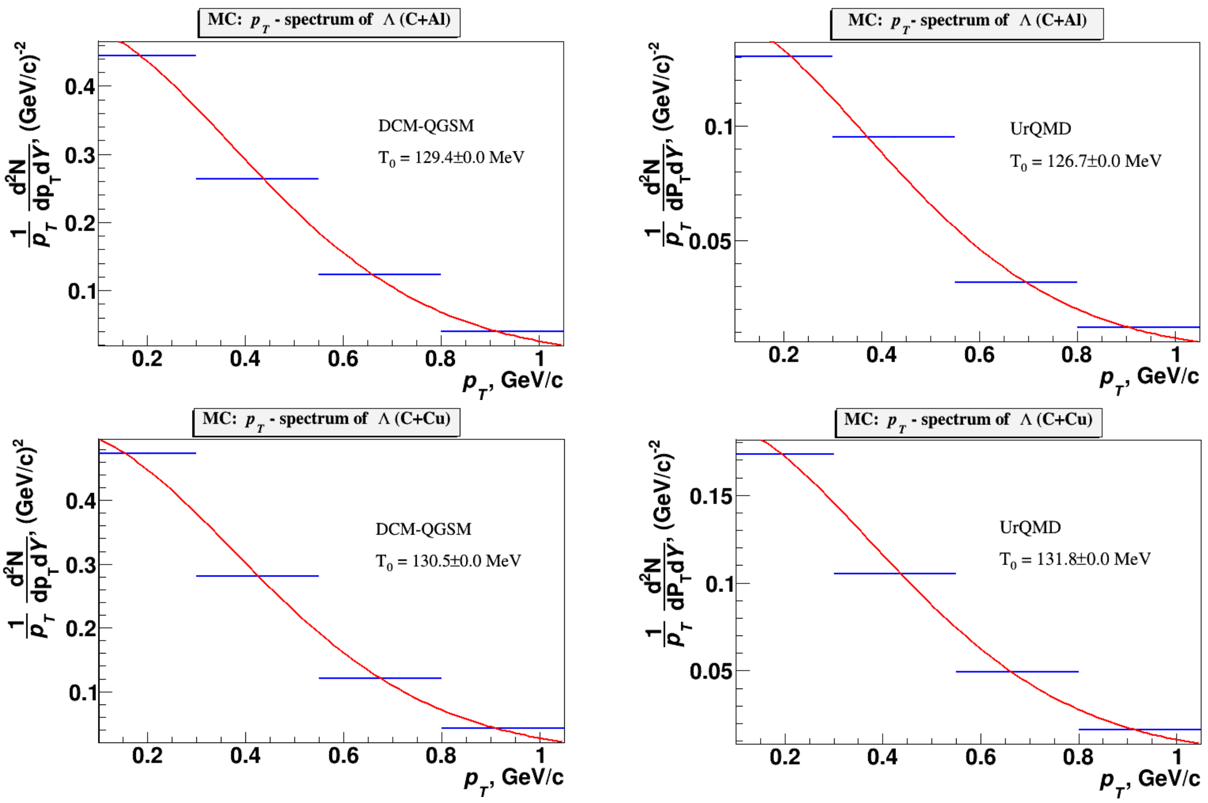

Fig. 24. Fit of the DCM-QGSM and URQMD *Λ* multiplicity spectra. The inverse slope parameter T_0 is shown, extracted from the fit.

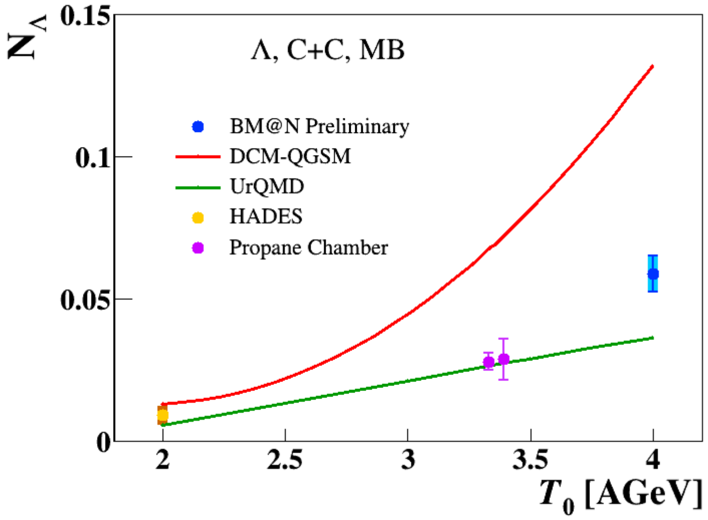

Fig.25. Energy dependence of *Λ* yields measured in different experiments. BM@N result is compared with data taken from [ArakelianCC], [ArmutCC], [HadesL0]. The predictions of the DCM-QGSM and UrQMD models are shown.

292

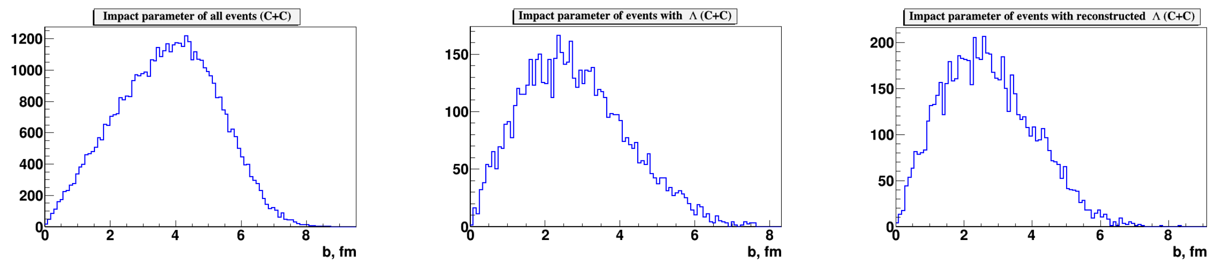

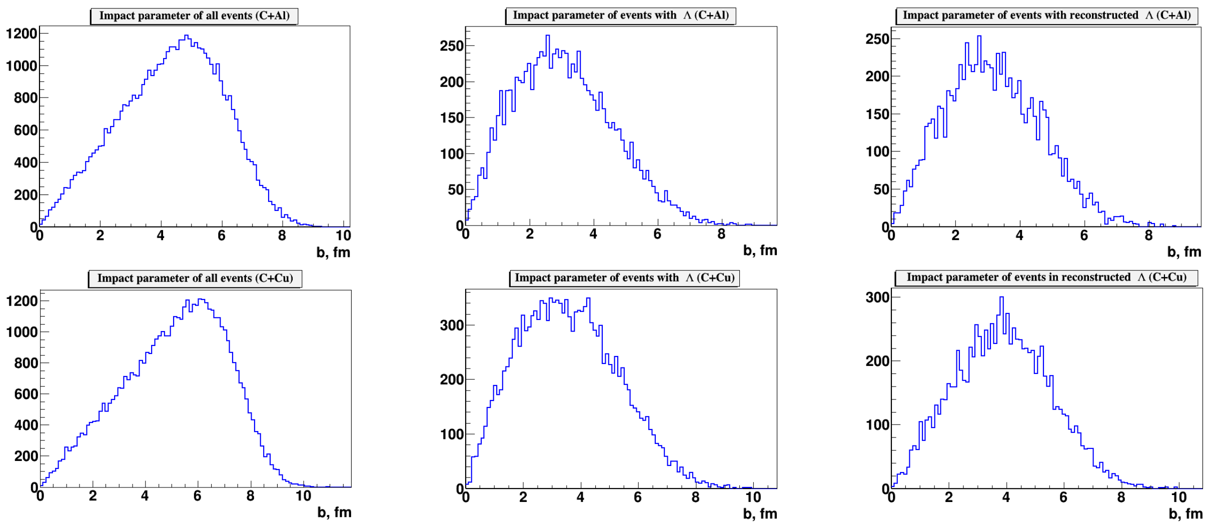

Fig. 26. Impact parameter distribution of all minimum bias events generated with the DCM-QGSM model (left). Impact parameter distribution of DCM-QGSM minimum bias events with generated *Λ* hyperons (center). Impact parameter distribution of DCM-QGSM minimum bias events with reconstructed *Λ* hyperons (right).

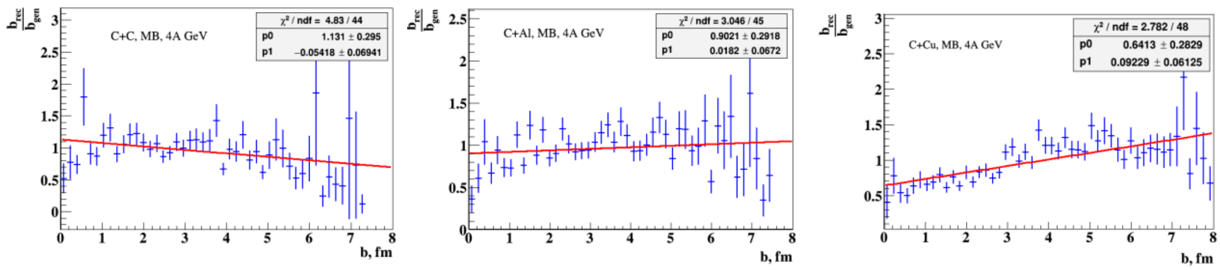

Fig.27. Ratio of impact parameter distributions for events with reconstructed *Λ* to events with generated *Λ* presented for *C+C*, *C+Al*, *C+Cu* interactions. Linear fit of the distributions is superimposed.